Analysis of natural variants of the Hepatitis C Virus Internal Ribosome Entry Site reveals that primary sequence plays a key role on cap-independent translation.

María Inés Barría[1,3], Angel González[5], Jorge Vera-Otarola[1,3]; Ursula León[1,3], Valeska Vollrath[1,3], Delphine Marsac[1,3], Octavio Monasterio[6], Tomás Pérez-Acle[5,7], Alejandro Soza[2,3], Marcelo López-Lastra[1,3,*].

(1) Laboratorio de Virología Molecular, Centro de Investigaciones Médicas, Facultad de Medicina, Pontificia Universidad Católica de Chile. (2) Departamento de Gastroenterología, Facultad de Medicina, Pontificia Universidad Católica de Chile. (3) Jeunes Equipes Associées à l'IRD y Nucleo Milenio de Inmunología e Inmunoterapia. (5) Centre for Bioinformatics (CBUC), Facultad de Ciencias Biológicas, Pontificia Universidad Católica de Chile. (6) Departamento de Biología, Facultad de Ciencias, Universidad de Chile. (7) Fundación Ciencia para la Vida.

***Corresponding author:** malopez@med.puc.cl (MLL), Laboratorio de Virología Molecular, Centro de Investigaciones Médicas, Pontificia Universidad Católica de Chile, Marcoleta 391, Santiago, Chile.

Running title: Characterization of natural variants of the HCV IRES.

Keywords: HCV, IRES.

ABSTRACT

The HCV internal ribosome entry site (IRES) spans a region of approximately 340 nt that encompasses most of the 5' untranslated region (5'UTR) of the viral mRNA and the first 24-40 nt of the core-coding region. To investigate the implication of altering the primary sequence of the 5'UTR on IRES activity, naturally occurring variants of the 5'UTR were isolated from clinical samples and analyzed. The impact of the identified mutations on translation was evaluated in the context of RLuc/FLuc bicistronic RNAs. Results show that depending on their location within the RNA structure, these naturally occurring mutations cause a range of effects on IRES activity. However, mutations within subdomain IIId hinder HCV IRES-mediated translation. In an attempt to explain these data, the dynamic behavior of the subdomain IIId was analyzed by means of Molecular Dynamics (MD) simulations. Despite the loss of function, MD simulations predicted that mutant G266A/G268U possesses a structure similar to the wt-RNA. This prediction was validated by analyzing the secondary structure of the isolated IIId RNAs by circular dichroism spectroscopy in the presence or absence of Mg^{2+} ions. These data strongly suggest that the primary sequence of subdomain IIId plays a key role in HCV IRES-mediated translation.

INTRODUCTION

Translation initiation of the vast majority of eukaryotic mRNAs occurs by a scanning mechanism, whereby the recognition of the mRNA's 5'cap structure (m^7GpppN) by eukaryotic translation initiation factors (eIFs) is followed by the binding of the 40S ribosomal subunit and scanning downstream to the initiation codon (1,2). The initiation factor eIF4F is responsible for positioning the 40S ribosomal subunit in proximity to the 5'cap structure. The 40S subunit is recruited to the mRNA as part of the 43S initiation complex, composed of the subunit bound to eIF2-GTP/Met-tRNAi (ternary complex), eIF1, eIF1A, and eIF3. Upon attachment to the vicinity of the cap the ribosomal subunit scans the mRNA in a 5' to 3' direction until the initiation codon is encountered leading to the formation of the 48S initiation complex in which the initiator AUG is base paired to the anticodon of the initiator tRNA. At this stage the eIFs are displaced from the 40S ribosomal subunit allowing the joining of the 60S subunit. Ribosomal subunit joining results in the formation of an 80S ribosome in which the initiator Met-tRNA is positioned in the ribosomal peptidyl (P) site (3,4). In contrast to the canonical mechanism of eukaryotic translation initiation, the Hepatitis C virus (HCV) mRNA uses an alternative ribosome recruitment mechanism by which the 40S ribosomal subunits directly binds to an RNA structure termed the HCV-internal ribosome entry site (IRES) (5-7). Ribosomal subunit binding to the HCV-IRES occurs in the absence of eIFs, in such a way that the initiation codon is placed in the immediate vicinity of the ribosomal P site not requiring ribosomal scanning (5,8,9). Subsequent addition of the ternary complex to the 40S/IRES complex is necessary and sufficient for the formation of the 48S complexes (5,6,8). Translation initiation factor eIF3 is not

needed for 48S complex formation (10), however it specifically binds to the HCV IRES and is required for subsequent joining of the 60S subunit to the 48S complex to form functional 80S ribosomes (5).

The HCV IRES spans a region of approximately 340 nt that encompasses most of the 5' untranslated region (UTR) of the viral mRNA and the first 24-40 nt of the core coding region (11,12). Under a physiological concentration of magnesium ions and in the absence of any additional factor, the 5'UTR is predicted to fold into a complex secondary/tertiary structure characterized by four major domains designated I to IV (13). Domain II, III and IV are necessary for IRES activity (14). Domain III is required for 40S ribosomal subunit and eIF3 binding (7,10,15,16). Domain II is responsible for the substantial conformational changes in 40S subunits induced by IRES binding (7), and for efficient eIF5-induced hydrolysis of eIF2-bound GTP in the 48S complexes assembled on the IRES (17). Domain IV contains the initiation codon and a portion of the Core protein open reading frame (ORF) (18).

Mutational analysis of the HCV IRES shows that the integrity of the higher order RNA structure is critical for HCV IRES activity (19-21). In an effort to further characterize the function of the different IRES structural domains on IRES function we undertook the challenge of identifying naturally occurring mutations within the HCV IRES of viral species present in clinical samples and evaluated their effect on translation in the context of a bicistronic RNA. In this study the 1b-IRES recovered from the HCV replicon pFK-I_{377}neo/NS3-3'/wt was used as the wild type (wt) IRES (22). Sequence analysis revealed that different isolates displayed diverse sets of mutations. The role of the each natural variant in IRES function was evaluated by introducing independent or

combined mutations within the sequence of the wt 1b-IRES. Our results show that depending on their location within the RNA structure, mutations cause a range of effects on IRES activity. Notably and in agreement with previous reports, we find that mutations within the IRES IIId subdomain have the most drastic effects on HCV IRES activity. In an attempt to further explain these observations, the dynamic behavior of the reference wt-IRES and of the specific mutations within the IRES subdomain IIId was analyzed by means of Molecular Dynamics (MD) simulations. Strikingly, MD analysis predicted that one of the isolated mutants in the IIId subdomain, namely mutant G266A/G268U, exhibited structural conservation with respect to the wt-IRES. This prediction was confirmed by circular dichroism (CD) spectroscopy. Together our results confirm the stringent structure/function relationship exhibited by the HCV IRES, but also suggest that the primary sequence of subdomain IIId plays a role in, and is required, for IRES-mediated translation initiation.

MATERIALS AND METHODS

Patients. 19 patients recruited from the outpatient clinic of the Hepatology Unit of the Clinical Hospital, Pontificia Universidad Católica de Chile (PUC) were included in this study. Protocols followed in this study were approved by the Ethical Review Board of the Faculty of Medicine, PUC. Donors signed a written consent form also approved by the Ethical Review Board of the Faculty of Medicine, PUC, before donating blood. Patient inclusion criteria have been described elsewhere (23). All patients were naïve to antiviral treatment. Both plasma and peripheral blood mononuclear cells (PBMC) were collected from each individual as previously described (23).

RNA purification. Total RNA was extracted using a protocol adapted from Chomczynski and Sacchi using a pellet of $5x10^6$ cells or 200 µl of plasma (24). RNA was resuspended in 30 µl of nuclease-free water. RNA concentrations were determined by spectrophotometry (GeneQuant, Pharmacia).

Plasmids. The HCV subgenomic replicon pFK-I_{377}neo/NS3-3'/wt (accession number: AJ242654) was kindly provided by Dr. R. Bartenschlager (University of Heidelberg, Germany) (22). Plasmid dl Δ-EMCV was kindly provided by Dr. P. Sarnow (Stanford University, USA) and corresponds to the Renilla luciferase-delta EMCV-Firefly luciferase vector that lacks an active IRES element (25,26). For the construction of vector DL-HCV 1b the HCV 1b IRES (nucleotide 14 to 383;AJ242654) was recovered by a one step reverse transcription (RT)-polymerase-chain reaction (PCR) using the SuperScript™ III one step RT-PCR system with Platinum® Taq DNA Polymerase

(Invitrogen) kit from the HCV subgenomic replicon pFK-I_{377}neo/NS3-3'/wt using primers P1-XhoI (5' GCCGCTCGAGTTGGGGGCGACACTCCACCATAGATC 3') and P4-EcoRI (5' CGGGGAATTCGTTACGTTTGGTTTTTCTTTGAGG 3'). The amplicon was cloned into the pGemT-easy vector (Promega). The pGemT plasmid DNA harboring the HCV 1b IRES was digested with XhoI and EcoRI and the recovered HCV IRES was cloned into the intercistronic region of the dual luciferase (DL) (RLuc/FLuc) vector described in Brasey et al. (2003) previously digested with XhoI and EcoRI to eliminate the Δ-EMCV-HIV-1 IRES sequences (25). HCV IRESes were recovered from total RNA purified from clinical samples by a one step RT-PCR using the SuperScript™ III one step RT-PCR system with Platinum® Taq DNA Polymerase (Invitrogen) kit using the P1-XhoI and P4-EcoRI primers and cloned directly into the pGemT-easy vector (Promega). pGemT plasmid harboring the HCV IRESes recovered from bacterial colonies were digested with XhoI and EcoRI and the viral IRES was cloned into the intercistronic region of the dual luciferase (DL) (RLuc/FLuc) as described above. All clones were sequenced (Macrogen Corp, USA) and aligned against the HCV prototype sequences using the CLUSTAL W program (27). A schematic representation of the biscistronic vectors used in this study is shown in figure 1A. For the generation of mutants C67T, A73G and G90A the DL-RLuc/FLuc vector harboring IRESes isolated from clinical samples containing each of the mutation were digested with XhoI and AgeI and ligated into the DL-RLuc/FLuc vector contained the HCV 1b IRES previously digested with XhoI and AgeI. For the generation of mutants A223G, U306C, C340T/G350A and U356A/A359G the DL-RLuc/FLuc vector harboring IRESes isolated from clinical samples containing the mutation were digested with AgeI and EcoRI and cloned into the

DL-RLuc/FLuc vector contained the HCV 1b IRES previously digested with AgeI and EcoRI. For the construction of the HCV IRES G82A/A172G and A119C/G331A double mutants the DL-RLuc/FLuc vector contained mutation A172G and G331A, respectively, obtained by PCR (as described below) were digested with AgeI and EcoRI and the fragment was ligated with the DL-RLuc/FLuc vector harboring the G82A and A119C changes, respectively, previously digested with AgeI and EcoRI. Point mutations G82A, A119C, G137T, A172G, A252G, G266A, G268T, G271A, G331A, A252G/G271A and G266A/G268T (primers mut 1 to 11, respectively) were introduced into the DL-RLuc/FLuc vector harboring the HCV 1b IRES following a PCR-based mutagenesis protocol (28), using three common oligonucleotides (renFw, P2anti and P1tag) and one mutation-specific oligonucleotide (mut 1-mut 11) for each mutant (Table 1). To obtain plasmids the DL-RLuc/FLuc vector harboring the mutant IRES two successive rounds of PCR using Platinum Taq DNA polymerase High Fidelity (Invitrogen) were conducted. The first round consists of two simultaneous PCR reactions one using the renFw and the different mut primers (containing the mutation, Table 1) while the second PCR was conducted using primers P1tag and P2anti (Table 1). Amplicons from each PCR reaction were purified, mixed and subjected to another round of PCR using the external primers renFw and P2anti (Table 1). The resulting PCR products were digested with XhoI and EcoRI and ligated into the intercistronic region of the DL-RLuc/FLuc vector previously digested with XhoI and EcoRI (see above). All constructs were verified by sequencing (Macrogen Corp, USA). Oligonucleotides used in this study are listed in Table 1.

In vitro transcription. Uncapped mRNAs were synthesized with T7 RNA polymerase (Fermentas). In brief, plasmids linearized with BamHI were used for in vitro transcription

in a 25µl final volume. The template DNA was digested with DNase I, and RNA was precipitated with 2.5M LiCl. RNA was resuspended in diethyl pyrocarbonate (DEPC)-treated water. Capped mRNAs were synthesized using the mMESSAGE mMACHINE High Yield Capped RNA Transcription Kits (Ambion, Applied Biosystems) following manufacturer's specifications. The poly(A) tailing kit (Ambion, Applied Biosystems) was used to add poly(A) tail to the capped mRNAs according to the manufacturer's specifications. RNA concentrations were determined spectrophotometrically and RNA integrity was monitored by electrophoresis on denaturing-agarose gels.

In vitro translation. For in vitro translations nuclease-treated rabbit reticulocyte lysate (35% RRL, Promega) were programmed with 8 ng/µl of RNA and reactions were performed at 90 min at 30°C, using salt conditions described in Svitkin et al. (2005). Human hepatoma cell line, Huh-7 (kindly provided by Dr. Bartenschlager) were grown as previously described (22), and Huh-7 based cell free translation extracts that were prepared according to previously published protocols (29). Huh-7 translation extracts (50%) were programmed with 60 ng/µl of RNA and translation was conducted for 90 min at 30°C. Renilla and Firefly Luciferase activities were measured in a single tube using the Dual-Luciferase® Reporter Assay System (Promega) on a Sirius luminometer (Berthold Detection Systems) according to the manufacturer's protocol.

Tranfection of Huh-7 cell. The 5'capped and 3'polyadenylated bicistronic RNAs harboring the mutant IRESes were transfected into Huh-7 cells using Lipofectamine 2000 Transfection Reagent (Invitrogen) according to the manufacturer's protocol. Huh-7 cells

were grown to 90% confluence in twelve-well tissue culture plates and transfected with a total of 400ng of capped/polyadenylated RNA. Cells were directly harvested with Passive Lysis 1X Buffer (Promega) 6-7 h post-transfection, and analyzed for luciferase as described above. The protein content of all samples was determined using the Bio-Rad Protein Assay (Bio-Rad Laboratories, Inc.).

HCV Genotyping. HCV genotyping of virus present in plasma and PBMCs was performed using the reverse-hybridization line probe assay, INNO-LiPA HCV II kit (Innogenetics, Ghent, Belgium) according to the manufacturer's instructions. Genotyping was confirmed by sequencing (Macrogen Corp, USA) and phylogenetic analysis as previously described (23)**.**

Molecular Dynamics (MD) Simulations. The HCV IRES IIId starting structure (wild type) was the best representative conformer of the experimental NMR data obtained by Lukavsky et al (PDBid: 1F84) (20). Mutants models (G266A, G268U and G266A/G268U) were generated from the wild type structure using the Nucleic Acid Modeling tool within Discovery Studio® research environment (Discovery Studio v1.7. Accelrys Inc*., San Diego* 2007). Hydrogen atoms were energy minimized by CHARMM (30,31), until a convergence of 0.001 kcal/mol•Å. During the minimization, the heavy atoms were held fixed and an implicit distance-dependent dielectric solvent model was employed (32). The wild type and mutant models were embedded in a periodic box [72 x 96 x 72] containing ~14800 water molecules. The water phase was extended to a distance of 25 Å from every solute atom and the RNA helix charges were neutralized by addition

of 29 Na+ counterions. Molecular dynamics simulations were carried out using the NAMD v 2.6 program (33). Nucleic acids parameters were taken from the Cornell force field (34), combined with the TIP3P water model parameters from CHARMM27 (35). Initial structures were energy minimized by conjugate gradient algorithm until a gradient tolerance of 0.001 was reached. After minimization, system temperature was raised in 30,000 steps to 298 K (0.01 K by step) by temperature reassignment method followed by 1ns of equilibration. During heating and equilibration, initial harmonic constraints on heavy atoms were gradually turned off in rounds of 500 ps to a final value of 0. Production runs were performed during 6ns at integration step of 1fs in the isothermic–isobaric thermodynamic ensemble at 298 K using the Settle algorithm on bonds involving water hydrogen atoms. Van der Waals interactions were truncated at 12Å, while electrostatic interactions were fully calculated with the Particle Mesh Ewald (PME) method. Non-bonded and long-range electrostatics forces were evaluated every 2 and 4 fs, respectively.

Structural Analysis. The calculation of the conformational space reachable by the individual nucleotides during the MD simulation was performed by the computation of the pseudotorsions angles between the two virtual bonds η ($C4'_{i-1}$−P_i−$C4'$−P_{i+1}) and θ (P_i−$C4'$−P_{i+1}−$C4'_{i+1}$) (36). Aromatic interactions between nucleotides were estimated by both; the distance between the centers of mass (COMs) of the aromatic bases, and by the α angle between the aromatic ring planes defined as the dot product of their normal vectors (37).

Circular dichroism spectroscopy measurements. Circular dichroism (CD) measurements were performed with a Jasco J-600 spectropolarimeter. 27 nt RNAs corresponding to the HCV stem-loop IIId wt (nt 253-279, HCV 1b) or mutants G266A, G268U and G266A/G268U used in these assays were synthesized by Integrated DNA Technologies (Coralville, USA). Samples contained 11-16 μM RNA in water or 1, 2 or 5 mM $MgCl_2$ were analyzed in a 1 mm CD quartz cuvette. RNA denaturation/renaturation experiments were performed as previously described (38). Wavelength scans were recorded from 200 to 300 nm at 50 nm/min at 25 ºC, using a 1 nm bandwidth, a 1 s response time. All the CD spectra were corrected by subtraction of the background for the spectrum obtained with water or $MgCl_2$ at the appropriate concentration. Spectra were averaged over four to five accumulations. Results were expressed as mean residue ellipticity, in degrees cm^2 $dmol^{-1}$ (38).

RESULTS

Isolation of HCV-IRES variants from viruses from the plasma and PBMCs of HCV chronically infected patients. Fifty four IRESes (nt 14-383) randomly isolated from clinical samples (plasma and PBMCs) obtained from 19 different HCV chronically infected individuals were cloned into a dual luciferase (DL) reporter construct containing an upstream *Renilla* luciferase gene (RLuc) and a downstream firefly luciferase gene (FLuc). In this context the HCV IRES activity was monitored using the FLuc activity as the readout, while the RLuc reporter gene serves as an upstream translational control (Fig. 1A). The RLuc/FLuc bicistronic vector harboring the type 1b IRES of the HCV subgenomic replicon pFK-I_{377}neo/NS3-3'/wt (22) was used as a positive control, while a DL-vectors containing a defective encephalomyocarditis virus (Δ-EMCV) IRES (Fig 1A), known to inhibit ribosome reinitiation and readthrough, inserted upstream of the FLuc reporter was used as a negative control (25,26).

Sequencing of the 5'UTR followed by alignment analysis (data not shown) revealed that 89% of the isolated IRESes corresponded to genotype 1b, 7% to genotype 3a, 2% to genotype 2a and 2% to genotype 5a (Fig. 1B). IRESes were considered natural variants if they presented at least one nucleotide difference when compared to the reference genotype. In this study the sequences from genotype 1b (AJ238799.1), 2a (D00944), 3a (D17763) and 5a (Y13184) were used as reference sequences. Natural variations in the nucleotide sequence of the HCV 5'UTR are referred to from here on as mutations. Sequence alignments showed that 14 out of the 48 1b isolated IRESes were identical in sequence to the control HCV-1b IRES (data not shown). In some cases similar mutant IRESes (IRES 8, IRES 9, IRES 12, IRES 13, IRES16, IRES 20, IRES 23,

and IRES 24 in Fig 1B) were isolated from different patients. In summary, only 28 of the initial 54 isolated IRESes, arbitrarily named 1-28, presented different sets of mutations when compared with the reference sequences (Fig. 1B).

In vitro activity of the natural variants of the HCV-IRES isolated from clinical samples. Next we evaluated the ability of the HCV IRESes recovered from clinical samples to drive translation in the RRL (Fig. 1B). The FLuc/RLuc ratio was used as an index of IRES activity, with the mean translation efficiency of the control HCV-1b IRES and the 14 1b-IRESes isolated from the clinical samples being arbitrarily set at 100% (+/- standard deviation). As shown in figure 1B, the relative translation efficiencies (RTEs) of the variant IRESes differed considerably, from 9 to 109% when compared with the HCV-1b control. The residual activity of the DL-ΔEMCV RNA, lacking IRES activity, is 7 % relative to the HCV-1b IRES. The RTE of the DL-ΔEMCV control vector was not subtracted from the RTE activities presented in figure 1B. These observations are therefore in concordance with results reported in previous studies (19-21,39-43), and confirm that not all mutations impacted equally on HCV-IRES activity.

Influence of the mutations identified in natural IRES variants on the activity of the HCV-1b IRES. To determine the influence of each of the mutations on viral IRES activity, substitutions were introduced into the HCV-1b IRES and their effect on translation was evaluated *in vitro*. We focused our study on nucleotide changes found in mutant IRESes with an impaired RTE (Fig. 1B). DL-vectors with the different mutant IRESes were named according to the nucleotide change with respect to the control HCV-

1b IRES. The ability of the different mutants to drive translation in RRL was evaluated using the FLuc/RLuc ratio as an index of IRES activity, with the mean translation efficiency of the control HCV-1b IRES being arbitrarily set to 100%. Figure 2A summarizes our findings. Mutations present in subdomain IIId are excluded from this scrutiny as they are independently analyzed in the next section.

In general mutations in domain II had a moderate effect on translation efficiency (RTE ranged from 95% to 52%; Figs. 1B and 2A). Transition U80C, located in the apical loop, had the most dramatic effect on IRES activity (RTE value of 52%). This finding is supported by a previous report showing a similar level of translation inhibition for the U80C and the U80A mutants (44). Mutation of nucleotide C104, shown to participate in a noncanonical base pair at the interaction surface of the IRES with the 40S ribosomal subunit (45), or of nucleotide A109 located at a Mg^{2+} binding site required to stabilize the conformation of subdomain IIa (45), had only a marginal effect on HCV IRES activity with RTE values of 95% and 71%, respectively (Fig. 1B).

Mutation G331A, predicted to destabilize a G331-C354 Watson-Crick interaction between the noncoding and coding portions of the viral IRES, in domain IV severely hindered HCV IRES translational activity (RTE of 28%; Fig. 2A). Other mutations found in domain IV, such as C340A (RTE of 104%) and G350A (RTE of 106%) did not significantly alter IRES activity (Fig. 1B). The natural variant A119C/G331A (IRES 7) had a RTE of 23% (Fig. 1B). Both mutations, when simultaneously introduced into the 1b-IRES consistently resulted in a translational activity of 21% (Fig 2A). However, on its own the A119C transversion merely reduced 1b-IRES activity to 72% (Fig. 2A), which is similar to the RTE of 84% observed for the natural variant IRES 6 (Fig 1B). Thus, we

conclude that the G331A transition is responsible for the diminished IRES activity presented by IRES 7 (Figs. 1B and 2A).

Activity of IRES 18 (G82A/A172G/ C127 and A207 insertions) was decreased by 73% (Fig. 1B). As insertion C127 (IRES 8; Fig. 1B) had marginal effects on HCV IRES activity, and mutation G82A/A207insertion had no effect on IRES activity (IRES 17, Fig. 1B), we predicted that mutation A172G alone was responsible for the low translational activity exhibited by IRES 18 (Fig. 1B). The A172G substitution is expected to disrupt the Watson-Crick A172-U227 pair in helix IIIb disturbing the network of bonds required for keeping the IIIabc junction together (19), disruption of which is expected to compromise the ability of the IRES to bind eIF3 and the ribosome (19). In agreement with this prediction overall translational activity was reduced to 30% when the A172G mutation was introduced in the context of the 1b-IRES (Fig. 2A). The low translational activity (RTE of 32%) of IRES G82A/A172G further validates our conclusion (Fig. 2A). Note that the A172G transition did not affect IRES activity as severely as the previously described A172U transvertion (19), suggesting that the conservation of a purine residue at position 172 might partially preserve the structure of the IIIabc junction.

HCV IRES activity is highly susceptible to mutations within subdomain IIId.

HCV IRES subdomain IIId, which spans nucleotides 253 to 279, forms the most extensive contact of the HCV IRES on the 40S subunit body (20,46). Consistent with this function mutations or deletions in subdomain IIId are reported to be deleterious to HCV IRES activity (20,40-42,47). Consistent with these findings, results presented in figure 1B show that IRESes 15 (C67U/A252G/G271A) and 25 (G137U/G266A/G268U), both

harboring mutations within subdomain IIId, displayed RTEs equivalent to the DL-ΔEMCV vector. To establish if indeed the mutations present in subdomain IIId were responsible for the low RTE displayed by IRESes 15 and 25 each mutation was independently introduced into the 1b-IRES. Under these conditions mutations C67U and G137U had only limited effects on HCV IRES activity (RTE of 88% and 64%, respectively; Fig. 2A). Therefore, on their own these mutations could not account for the lack of translational activity of IRESes 15 and 25. However, in agreement with previous reports (10,20,40-42), point mutations A252G, G266A, G268U, and G271A (Fig. 2B), diminished HCV IRES activity to 47%, 14%, 14%, and 59%, respectively (Fig. 2C). The dual substitution mutants A252G/G271A and G266A/G268U also showed important reductions in translational activity (RTE of 15% and 14% respectively) (Fig. 2C).

Biochemical reconstitution of the initiation process on the HCV IRES revealed that formation of the IRES-40S-eIF3 ternary preinitiation complex is independent of other eIFs (15). However, the HCV IRES requires cellular proteins for optimal translational activity (48,49). One plausible explanation for the impairment in translational activity observed for the different IIId mutants is that HCV IRES transacting factor(s) are absent from, or available in limiting concentrations only in the RRL. To assess this possibility, translation efficiencies of the different IIId mutants were evaluated in Huh-7 cell derived translation extracts (29). Huh-7 cells represent a well characterized human hepatocellular carcinoma cell line known to support replication of the HCV subgenomic replicon and the JFH1 genotype 2a HCV strain (22,50). In Huh-7 cell based translation extracts mutants A252G, G266A, G268U, G271A, A252G/G271A, and G266A/G268U exhibited a drastic reduction in translational activity (Fig. 2C). The

apparent discrepancy between the results obtained in RRL (nuclease-treated) versus Huh-7 cell based translation extracts is likely due to the presence of endogenous mRNA in the latter, leading to competition for the translational apparatus and to lower translational activity.

To further challenge our observations we next assessed whether mutations within HCV IRES subdomain IIId reduce translation in cells. The rational for this experiment was derived from the report of Otto and Puglisi (2004), who reported that deletion of the IIId loop-E motif diminished HCV IRES mediated translation in the RRL but not in cells (6). To this end, the *in vitro* generated, capped and polyadenylated RNA corresponding to the DL-vectors harboring the wt- or the mutant-IRESes were transfected into Huh-7 cell lines (Fig. 2D). Expression of the first cistron, RLuc, was used as an indicator of transfection efficiency (Fig. 2D). Consistent with the data generated *in vitro*, mutations within subdomain IIId totally impaired HCV IRES activity in Huh-7 cells (Fig. 2D).

Molecular Dynamics (MD) simulations of HCV IRES subdomain IIId.

The overall structure of subdomain IIId is well defined by NMR (20,51). Thus, to obtain insights into the molecular mechanisms by which mutations in the loop region of subdomain IIId might hinder HCV IRES activity, we used the NMR data to produce *in silico* models of HCV IRES wild type and mutant IIId subdomain (Fig. 3A). The dynamic behavior of these models was studied by means of MD simulations of the wt- and mutant-IIId subdomains, which exhibited a broad structural conservation of the average features that characterize the IIId domain (Fig. 3A). Consistent with both the NMR data and previous MD simulation reports (20,52), the average root mean squared deviation

(RMSD) values per nucleotide were less than 3Å in all but the hexanucleotide (HN) hairpin loop region (Fig. 3B). Strikingly, the MD simulations predicted that the G266A, G268U and G266A/G268U mutations only generate a local conformational change in the apical HN loop region (Fig. 3A and B). When comparing the HN loop regions of the four MD models, mutant G268U appears to be the most disordered while the G266A/G268U double mutant exhibits higher stability (Fig. 3A and B).

Some features within the HN loop region such as the base stacking between nucleotides 266 and 267, the location of nucleotide 268 above the major groove and the exposure of U269 to the solvent phase resulted in common elements to all the analyzed structures (Fig. 3B). The most noticeable difference between the four MD models is the conformational preference for nucleotide U265 (Fig. 3B and C). NMR shows that in the wt-context U265 is highly disordered in comparison to the three guanosine residues (20). However, an analysis of pseudotorsion angles of the different MD models underscores the restricted conformation of U265 in the double mutant, highlighting clear differences between the single mutants and the wild type model (Fig. 3C) (36). These results further stress the higher stability of the G266A/G268U double mutant when compared to both the single mutants and to the wt-IIId MD models (Fig. 3). Flexibility of U265 in the single mutants allows this nucleotide to locate towards the minor groove enabling the establishment of an aromatic stacking interaction with the nucleotide at position 266 (Fig. 3D). This interaction, albeit observed only transiently during data collection (not shown) is able to modify the local environment around nt 266 and 267, both important for IRES-40S subunit interaction (20). The increased stability in the HN hairpin region exhibited by the G266A/G268U double mutant can be explained by a noncanonical hydrogen bond

interaction established between 2´-hydroxyl groups from nucleotides U264 and ribose U268 in the major groove of the structure (Fig. 3D and E). This type of base-ribose interaction is known to stabilize RNA structures (53) and most probably restores, to some extent, the loop structure that is normally stabilized by a trans-wobble U264-G268 base pair (51). These data highlight the significance of the trans-wobble U264-G268 base pair in the structure conservation of subdomain IIId.

Circular dichroism spectroscopy studies of the HCV IRES subdomain IIId.

The MD data predicted that wt- and G266A/G268U mutant IIId folding was similar (Fig. 3A). To challenge this prediction, we studied the circular dichroism spectra (CD) of a synthetic 27-nt RNA corresponding to the HCV IRES subdomain IIId (nt 253-279) (20). CD is mostly based on a comparative analysis between different structures, but provides essential information about the conformational properties of nucleic acids in solution (54). This experimental approach has previously been used to study the folding of the HCV IRES upon thermal melting (38). Controversy remains over the effect of Mg^{2+} ions on IRES structure (38,40,51), thus we first evaluated by CD the effect of Mg^{2+} ions (0, 1, 2, or 5 mM) on the folding of subdomain IIId upon thermal melting followed by renaturation as previously described (38). The selection of ion concentrations was based on reports showing that a folding transition of the HCV IRES occurs at a 1 mM Mg^{2+} (40), *in vitro* HCV IRES activity is optimal at 2 mM Mg^{2+} (40,55), and HCV IRES is functional, albeit to a lesser extent, at 5 mM Mg^{2+} (38,56). Before conducting the assays we established the effect of Mg^{2+} ions on RNA aggregation. Consistent with previous reports (38,40), we found that all synthetic RNAs resolved as a sharp single

band in native polyacrylamide gel electrophoresis in the presence of 0, 1, 2 or 5 mM Mg^{2+}, indicating an absence of RNA aggregation in these experimental conditions (data not shown).

The CD spectra of renatured wt-IIId RNA revealed that, in isolation, the renaturation of subdomain IIId (a synthetic 27-nt RNA) following thermal melting was ion-dependent (Fig. 4A). The CD spectra of the wt-IIId and mutant-IIId RNAs exhibited two major peaks centered at 260 and 205 nm. These peaks are due to π-π electron transitions in the stacked planar bases, influenced by asymmetric 3'-endo sugar rings (38,54). The wavelengths of the peak are characteristic of RNA in an A-form helical conformation (38). Upon thermal melting the CD spectra of the wt-IIId significantly changed when RNA was renatured in presence of Mg^{2+} ions (Fig. 4A). The change in the CD spectra are assumed to reflect the conformational change in the RNA induced by Mg^{2+} binding (38,54). The magnitude of peaks at 260 and 205 nm increased when 1 and 2 mM $MgCl_2$ was added, indicating increased helix structure and base stacking. In agreement with previous reports a folding transition occurred between 0 and 1 mM Mg^{2+} (Fig. 4A) (40). The structure of the subdomain IIId was maintained at 2 mM Mg^{2+}, while at 5 mM Mg^{2+} 260 and 205 nm peaks decreased relative to those at 1 and 2 mM Mg^{2+} (Fig. 4A). Even though the effect of 5mM Mg^{2+} on the conformational changes of subdomain IIId cannot be readily explained, data were highly reproducible in repeat experiments. Taken together, these data stress that upon thermal denaturation Mg^{2+} ions are required to permit folding of subdomain IIId of the HCV IRES.

We next studied the CD renaturation spectra of the G266A, G268U and G266A/G268U mutant RNAs in the presence of 2 mM $MgCl_2$ and compared them to the

renaturation spectra of the wt-IIId RNA. Ion concentration affected the CD spectra of these RNAs in a dissimilar manner indicating, in the case of the native and the G266A/G268U double mutant RNAs, an increase in base stacking that might represent greater helix stability (Fig. 4B). Moreover and consistent with the MD models (Fig.3), the CD spectra of the G266A/G268U double mutant strikingly resembled those of the wt-IIId, yet both CD spectra clearly differed from those obtained for the G266A and G268U single mutants, suggesting dissimilar RNA structures. These observations are in agreement with previous reports showing that a G266C mutation alters the ion-dependent structure of the HCV IRES (40). Therefore the structural differences between both single mutants and the wt-IIId domain may be responsible for the reduced IRES activity (Fig. 2C).

Because the CD spectra obtained for the G266A/G268U double mutant resembled those of the wt-IIId at 2 mM Mg^{2+} (Fig. 4B) we decided to establish if this structural similarity was maintained at different Mg^{2+} concentrations (Fig. 5). Noticeably, the double mutant and wt-IIId domains exhibited similar CD renaturation spectra in either the absence or the presence of different concentrations of Mg^{2+} ions indicating that, in isolation, the wt-IIId and G266A/G268U double mutant subdomain IIId share similar structural features (Fig. 5). Overall the evidence presented herein strongly suggests that mutations G266A/G268U hinder IRES activity without altering the structure of subdomain IIId.

DISCUSSION.

The molecular mechanisms that determine the function of viral IRESes are not clearly understood. In the case of the HCV IRES the demonstration that many domain mutations resulting in reduced protein synthesis can be restored by compensatory mutations suggests that the IRES structure is required to initiate protein synthesis (9,13,19-21,57-59). Also, mutations in the loop regions of subdomains IIIc and IIIe indicate that the function of the HCV IRES relies, to some degree, on its primary sequence (39,60). In this study, we have sought to further understand the relation between IRES structure and function by analyzing natural variants of the HCV IRES isolated from clinical samples. Results of this study not only confirm the stringent structure/function relationship exhibited by the HCV IRES but also highlight the importance of the primary sequence of subdomain IIId in the translation of the viral mRNA.

Natural IRES variants of HCV genotypes 1b, 2a, 3a, and 5a were isolated from clinical samples (Fig. 1B). Sequencing analysis allowed the identification of naturally occurring mutations within the isolated IRESes (Fig. 1B). Interestingly, a number of the variants identified herein have been previously found in clinical samples (39,41,61-63). The effect of the naturally occurring mutations on IRES-driven translation was evaluated by introducing each one in the wt-1b IRES background (Fig. 2 and 3). Consistent with previous reports our results show that mutations within domains II and IV (Figs. 1B and 2A) have a moderate effect on translation efficiency while mutations in domain III (Figs. 2B,C, and D) diminished the activity of the HCV IRES. Interestingly, among the natural IRES variants isolated in this study we identified mutations within subdomain IIId that hindered IRES activity without altering the local folding of this subdomain (Figs. 2-5).

To further understand how mutations within loop structures could diminish IRES activity we performed molecular dynamic (MD) simulations on a model of the IIId domain developed on the basis of previously reported NMR data (20,51). Unexpectedly, MD simulations predicted that one of the tested IRES mutants, namely the G266A/G268U double mutant, shared similar structural features with the wt-IIId subdomain (Fig. 3). This prediction was confirmed by circular dichroism (CD) spectrometry analysis at different Mg^{2+} ion concentrations (Figs. 4 and 5). Together these observations suggest that the G266A/G268U double mutant folded into a structure similar to the wt-IIId, yet the 1b-IRES that harbors these mutations lacks the ability to initiate translation. Consequently, it can be concluded that the primary sequence of subdomain IIId is required for optimal translation from the HCV IRES. Interestingly, the importance of the primary sequence in HCV IRES function does not seem to be restricted to the HN loop of subdomain IIId. A previous study describes that IRES activity is hindered by mutations within loops IIIc but that IRES folding is not altered (39). This sensitivity to primary sequence is not however a feature common to all loop structures within the HCV IRES. In agreement with previous reports (39,58,64) we describe insensitivity to mutational changes within the subdomain IIIb loop (IRES 9, Fig. 1B), suggesting that in this case the primary sequence does not play a role in HCV IRES function.

Several models can be proposed to explain our observations. One possibility is that the primary sequence of the HN loop is important for preserving long distance RNA-RNA interactions of subdomain IIId with subdomians IIIe and IIIf (40), or between subdomain IIId and domain II (65). This option is consistent with data showing that subdomain IIId participates in IRES structural transitions affected by ions (38,40), and

with observation indicating that mutations within this subdomain induce structural reorganization of the HCV IRES (42). Considering that subdomain IIId participates in the docking of the 40S ribosomal subunit, an alternative possibility is that mutations within this subdomain inhibit 40S ribosomal subunit binding to the IRES. In agreement with this option a previously described IRES mutant [G(266–268)C] exhibited reduced 40S binding affinity and resultant block of 48S preinitiation complex formation (8,10). However, our first model fails to explain data generated using IRES mutant G(266–268)A (6,20). When compared to the wt-IRES the G(266–268)A mutant does not exhibit an altered secondary structure. The mutations only marginally alter the binding capacity of the 40S ribosomal subunit, yet, consistent with our findings nucleotide substitutions cause a severe translation defect (6,20). It would therefore seem that preserving the fold of subdomain IIId (G(266–268)A) is not sufficient to ensure IRES-activity (6,20).

After binding, the subsequent docking of the IRES ORF into the mRNA cleft requires some degree of structure melting. For example, nucleotide substitutions predicted to enhance the stability of the domain IV stem-loop are deleterious to translation initiation both *in vitro* and *in vivo* (18). Additional mutations that destabilize the stem-loop restored translation to a normal level (18). Thus, melting of some RNA domains may be required for translation initiation to progress beyond 40S binding. The predicted stabilization of subdomain IIId in the G266A/G268U double mutant (Fig. 3) may lock the 40S ribosomal subunit into a conformation which inhibits further steps of the initiation or the elongation process. Alternatively, stabilization of subdomain IIId may prevent the correct positioning of the 40S ribosomal subunit over the IRES element (6,66). This is of special relevance considering that correct binding of the 40S ribosomal subunit is required for

the IRES to position the viral mRNA in the ribosomal P site without the assistance of canonical initiation factors.

In conclusion the presented mutational and structural studies indicate that full functionality of the HCV IRES relies on both its primary sequence and secondary structure. Based on the stringent relationship between sequence/structure/function of subdomain IIId and on the fact that it is highly conserved among HCV genotypes it seems reasonable to propose that this subdomain of the HCV IRES holds promise as a specific target for the development of novel antiviral strategies directed against viral protein synthesis.

FUNDING

This study was supported by a grant from the Institut de Recherche pour le Développement (IRD) through its Jeunes Equipes Associées à l'IRD International Program and by the Comisión Nacional de Investigación Científica y Tecnológica, Gobierno de Chile, CONICYT through grant FONDECYT N^{o} 1080323 to A. S. and MLL. MIB was supported by a CONICYT and an IRD doctoral fellowship. AG and JV-O are recipients of a CONICYT and MECESUP-USACH doctoral fellowships, respectively. DM was initially supported through a Millennium Nucleus on Immunology and Immunotherapy (NMII) Post-doctoral fellowship and currently holds a FONDECYT N^{o}3085029 Post-doctoral fellowship.

ACKNOWLEDGEMENTS

We thank Drs. JL. Darlix and M. Rau for critical reading of the manuscript, Drs. R. Bartenschlager (University of Heidelberg) and P. Sarnow (Stanford University) for kindly providing plasmids, cells, and reagents used in this study. We thank Dr. J. Winkler (University of Vienna) for helpful discussion regarding the CD data. We appreciate the help of Nurse M. Velasco during sample collection. We thank C. Pasquot for her administrative assistance. MIB conducted this work as part of her PhD thesis, Programa de Doctorado en Ciencias Biológicas, Facultad de Ciencias, Universidad de Chile. AG is student of the Programa de Doctorado en Biotecnología, Universidad Andres Bello and JV-O is student of the Programa de Doctorado en Microbiología, Universidad de Santiago de Chile.

REFERENCES

1. Pestova, T.V., Kolupaeva, V.G., Lomakin, I.B., Pilipenko, E.V., Shatsky, I.N., Agol, V.I. and Hellen, C.U. (2001) Molecular mechanisms of translation initiation in eukaryotes. *Proc Natl Acad Sci U S A*, **98**, 7029-7036.
2. Lopez-Lastra, M., Rivas, A. and Barria, M.I. (2005) Protein synthesis in eukaryotes: the growing biological relevance of cap-independent translation initiation. *Biol Res*, **38**, 121-146.
3. Pestova, T.V., Lomakin, I.B., Lee, J.H., Choi, S.K., Dever, T.E. and Hellen, C.U. (2000) The joining of ribosomal subunits in eukaryotes requires eIF5B. *Nature*, **403**, 332-335.
4. Unbehaun, A., Borukhov, S.I., Hellen, C.U. and Pestova, T.V. (2004) Release of initiation factors from 48S complexes during ribosomal subunit joining and the link between establishment of codon-anticodon base-pairing and hydrolysis of eIF2-bound GTP. *Genes Dev*, **18**, 3078-3093.
5. Pestova, T.V., Shatsky, I.N., Fletcher, S.P., Jackson, R.J. and Hellen, C.U. (1998) A prokaryotic-like mode of cytoplasmic eukaryotic ribosome binding to the initiation codon during internal translation initiation of hepatitis C and classical swine fever virus RNAs. *Genes Dev*, **12**, 67-83.
6. Otto, G.A. and Puglisi, J.D. (2004) The pathway of HCV IRES-mediated translation initiation. *Cell*, **119**, 369-380.
7. Spahn, C.M., Kieft, J.S., Grassucci, R.A., Penczek, P.A., Zhou, K., Doudna, J.A. and Frank, J. (2001) Hepatitis C virus IRES RNA-induced changes in the conformation of the 40s ribosomal subunit. *Science*, **291**, 1959-1962.
8. Ji, H., Fraser, C.S., Yu, Y., Leary, J. and Doudna, J.A. (2004) Coordinated assembly of human translation initiation complexes by the hepatitis C virus internal ribosome entry site RNA. *Proc Natl Acad Sci U S A*, **101**, 16990-16995.
9. Reynolds, J.E., Kaminski, A., Carroll, A.R., Clarke, B.E., Rowlands, D.J. and Jackson, R.J. (1996) Internal initiation of translation of hepatitis C virus RNA: the ribosome entry site is at the authentic initiation codon. *Rna*, **2**, 867-878.
10. Kieft, J.S., Zhou, K., Jubin, R. and Doudna, J.A. (2001) Mechanism of ribosome recruitment by hepatitis C IRES RNA. *Rna*, **7**, 194-206.
11. Reynolds, J.E., Kaminski, A., Kettinen, H.J., Grace, K., Clarke, B.E., Carroll, A.R., Rowlands, D.J. and Jackson, R.J. (1995) Unique features of internal initiation of hepatitis C virus RNA translation. *Embo J*, **14**, 6010-6020.
12. Tsukiyama-Kohara, K., Iizuka, N., Kohara, M. and Nomoto, A. (1992) Internal ribosome entry site within hepatitis C virus RNA. *J Virol*, **66**, 1476-1483.
13. Honda, M., Ping, L.H., Rijnbrand, R.C., Amphlett, E., Clarke, B., Rowlands, D. and Lemon, S.M. (1996) Structural requirements for initiation of translation by internal ribosome entry within genome-length hepatitis C virus RNA. *Virology*, **222**, 31-42.
14. Fraser, C.S. and Doudna, J.A. (2007) Structural and mechanistic insights into hepatitis C viral translation initiation. *Nat Rev Microbiol*, **5**, 29-38.
15. Sizova, D.V., Kolupaeva, V.G., Pestova, T.V., Shatsky, I.N. and Hellen, C.U. (1998) Specific interaction of eukaryotic translation initiation factor 3 with the 5'

nontranslated regions of hepatitis C virus and classical swine fever virus RNAs. *J Virol*, **72**, 4775-4782.
16. Buratti, E., Tisminetzky, S., Zotti, M. and Baralle, F.E. (1998) Functional analysis of the interaction between HCV 5'UTR and putative subunits of eukaryotic translation initiation factor eIF3. *Nucleic Acids Res*, **26**, 3179-3187.
17. Locker, N., Easton, L.E. and Lukavsky, P.J. (2007) HCV and CSFV IRES domain II mediate eIF2 release during 80S ribosome assembly. *Embo J*, **26**, 795-805.
18. Honda, M., Brown, E.A. and Lemon, S.M. (1996) Stability of a stem-loop involving the initiator AUG controls the efficiency of internal initiation of translation on hepatitis C virus RNA. *Rna*, **2**, 955-968.
19. Kieft, J.S., Zhou, K., Grech, A., Jubin, R. and Doudna, J.A. (2002) Crystal structure of an RNA tertiary domain essential to HCV IRES-mediated translation initiation. *Nat Struct Biol*, **9**, 370-374.
20. Lukavsky, P.J., Otto, G.A., Lancaster, A.M., Sarnow, P. and Puglisi, J.D. (2000) Structures of two RNA domains essential for hepatitis C virus internal ribosome entry site function. *Nat Struct Biol*, **7**, 1105-1110.
21. Collier, A.J., Gallego, J., Klinck, R., Cole, P.T., Harris, S.J., Harrison, G.P., Aboul-Ela, F., Varani, G. and Walker, S. (2002) A conserved RNA structure within the HCV IRES eIF3-binding site. *Nat Struct Biol*, **9**, 375-380.
22. Lohmann, V., Korner, F., Koch, J., Herian, U., Theilmann, L. and Bartenschlager, R. (1999) Replication of subgenomic hepatitis C virus RNAs in a hepatoma cell line. *Science*, **285**, 110-113.
23. Barria, M.I., Vera-Otarola, J., Leon, U., Vollrath, V., Marsac, D., Riquelme, A., Lopez-Lastra, M. and Soza, A. (2008) Influence of extrahepatic viral infection on the natural history of hepatitis C. *Ann Hepatol*, **7**, 136-143.
24. Chomczynski, P. and Sacchi, N. (1987) Single-step method of RNA isolation by acid guanidinium thiocyanate-phenol-chloroform extraction. *Anal Biochem*, **162**, 156-159.
25. Brasey, A., Lopez-Lastra, M., Ohlmann, T., Beerens, N., Berkhout, B., Darlix, J.L. and Sonenberg, N. (2003) The leader of human immunodeficiency virus type 1 genomic RNA harbors an internal ribosome entry segment that is active during the G2/M phase of the cell cycle. *J Virol*, **77**, 3939-3949.
26. Wilson, J.E., Powell, M.J., Hoover, S.E. and Sarnow, P. (2000) Naturally occurring dicistronic cricket paralysis virus RNA is regulated by two internal ribosome entry sites. *Mol Cell Biol*, **20**, 4990-4999.
27. Thompson, J.D., Higgins, D.G. and Gibson, T.J. (1994) CLUSTAL W: improving the sensitivity of progressive multiple sequence alignment through sequence weighting, position-specific gap penalties and weight matrix choice. *Nucleic Acids Res*, **22**, 4673-4680.
28. Mikaelian, I. and Sergeant, A. (1992) A general and fast method to generate multiple site directed mutations. *Nucleic Acids Res*, **20**, 376.
29. Svitkin, Y.V., Pause, A., Lopez-Lastra, M., Perreault, S. and Sonenberg, N. (2005) Complete translation of the hepatitis C virus genome in vitro: membranes play a critical role in the maturation of all virus proteins except for NS3. *J Virol*, **79**, 6868-6881.

30. Brooks, B.R., Bruccoleri, R.E., Olafson, B.D., States, D.J., Swaminathan, S. and Karplus, M. (1983) CHARMM: A program for macromolecular energy minimization and dynamics calculations. *J. Comp. Chem.*, 187-217.
31. Momany, F.A. and Rone, R. (1992) Validation of the General Purpose QUANTA3.2/CHARMm Force Field. *Journal of Computational Chemistry*, **13**, 888-900.
32. Mazur, J. and Jernigan, R.L. (1991) Distance-dependent dielectric constants and their application to double-helical DNA. *Biopolymers*, **31**, 1615-1629.
33. Phillips, J.C., Braun, R., Wang, W., Gumbart, J., Tajkhorshid, E., Villa, E., Chipot, C., Skeel, R.D., Kale, L. and Schulten, K. (2005) Scalable molecular dynamics with NAMD. *J Comput Chem*, **26**, 1781-1802.
34. Cornell, W.D., Cieplak., P., Bayley., C.I., Gould., I.R., Merz., K.M., Ferguson., D.M., Spellmeyer., D.C., Fox., T., Caldwell., J.W. and Kollman., P.A. (1995) A second generation force field for simulation of proteins, nucleic acids and organic molecules. *J. Am. Chem. Soc*, **117**, 5179-5197.
35. Foloppe, N. and MacKerell, A.D. (2000) All-Atom Empirical Force Field for Nucleic Acids: 2) Parameter Optimization Based on Small Molecule and Condensed Phase Macromolecular Target Data. *J. Comp. Chem.*, **21**, 86-104.
36. Duarte, C.M. and Pyle, A.M. (1998) Stepping through an RNA structure: A novel approach to conformational analysis. *J Mol Biol*, **284**, 1465-1478.
37. Hunter, C.A., Singh, J. and Thornton, J.M. (1991) Pi-pi interactions: the geometry and energetics of phenylalanine-phenylalanine interactions in proteins. *J Mol Biol*, **218**, 837-846.
38. Vos, S., Berrisford, D.J. and Avis, J.M. (2002) Effect of magnesium ions on the tertiary structure of the hepatitis C virus IRES and its affinity for the cyclic peptide antibiotic viomycin. *Biochemistry*, **41**, 5383-5396.
39. Tang, S., Collier, A.J. and Elliott, R.M. (1999) Alterations to both the primary and predicted secondary structure of stem-loop IIIc of the hepatitis C virus 1b 5' untranslated region (5'UTR) lead to mutants severely defective in translation which cannot be complemented in trans by the wild-type 5'UTR sequence. *J Virol*, **73**, 2359-2364.
40. Kieft, J.S., Zhou, K., Jubin, R., Murray, M.G., Lau, J.Y. and Doudna, J.A. (1999) The hepatitis C virus internal ribosome entry site adopts an ion-dependent tertiary fold. *J Mol Biol*, **292**, 513-529.
41. Laporte, J., Malet, I., Andrieu, T., Thibault, V., Toulme, J.J., Wychowski, C., Pawlotsky, J.M., Huraux, J.M., Agut, H. and Cahour, A. (2000) Comparative analysis of translation efficiencies of hepatitis C virus 5' untranslated regions among intraindividual quasispecies present in chronic infection: opposite behaviors depending on cell type. *J Virol*, **74**, 10827-10833.
42. Jubin, R., Vantuno, N.E., Kieft, J.S., Murray, M.G., Doudna, J.A., Lau, J.Y. and Baroudy, B.M. (2000) Hepatitis C virus internal ribosome entry site (IRES) stem loop IIId contains a phylogenetically conserved GGG triplet essential for translation and IRES folding. *J Virol*, **74**, 10430-10437.
43. Odreman-Macchioli, F., Baralle, F.E. and Buratti, E. (2001) Mutational analysis of the different bulge regions of hepatitis C virus domain II and their influence on internal ribosome entry site translational ability. *J Biol Chem*, **276**, 41648-41655.

44. Kalliampakou, K.I., Psaridi-Linardaki, L. and Mavromara, P. (2002) Mutational analysis of the apical region of domain II of the HCV IRES. *FEBS Lett*, **511**, 79-84.
45. Lukavsky, P.J., Kim, I., Otto, G.A. and Puglisi, J.D. (2003) Structure of HCV IRES domain II determined by NMR. *Nat Struct Biol*, **10**, 1033-1038.
46. Kolupaeva, V.G., Pestova, T.V. and Hellen, C.U. (2000) An enzymatic footprinting analysis of the interaction of 40S ribosomal subunits with the internal ribosomal entry site of hepatitis C virus. *J Virol*, **74**, 6242-6250.
47. Odreman-Macchioli, F.E., Tisminetzky, S.G., Zotti, M., Baralle, F.E. and Buratti, E. (2000) Influence of correct secondary and tertiary RNA folding on the binding of cellular factors to the HCV IRES. *Nucleic Acids Res*, **28**, 875-885.
48. Costa-Mattioli, M., Svitkin, Y. and Sonenberg, N. (2004) La autoantigen is necessary for optimal function of the poliovirus and hepatitis C virus internal ribosome entry site in vivo and in vitro. *Mol Cell Biol*, **24**, 6861-6870.
49. Kim, J.H., Paek, K.Y., Ha, S.H., Cho, S., Choi, K., Kim, C.S., Ryu, S.H. and Jang, S.K. (2004) A cellular RNA-binding protein enhances internal ribosomal entry site-dependent translation through an interaction downstream of the hepatitis C virus polyprotein initiation codon. *Mol Cell Biol*, **24**, 7878-7890.
50. Wakita, T., Pietschmann, T., Kato, T., Date, T., Miyamoto, M., Zhao, Z., Murthy, K., Habermann, A., Krausslich, H.G., Mizokami, M. *et al.* (2005) Production of infectious hepatitis C virus in tissue culture from a cloned viral genome. *Nat Med*, **11**, 791-796.
51. Klinck, R., Westhof, E., Walker, S., Afshar, M., Collier, A. and Aboul-Ela, F. (2000) A potential RNA drug target in the hepatitis C virus internal ribosomal entry site. *Rna*, **6**, 1423-1431.
52. Golebiowski, J., Antonczak, S., Di-Giorgio, A., Condom, R. and Cabrol-Bass, D. (2004) Molecular dynamics simulation of hepatitis C virus IRES IIId domain: structural behavior, electrostatic and energetic analysis. *J Mol Model*, **10**, 60-68.
53. Tamura, M. and Holbrook, S.R. (2002) Sequence and structural conservation in RNA ribose zippers. *J Mol Biol*, **320**, 455-474.
54. Sosnick, T.R., Fang, X. and Shelton, V.M. (2000) Application of circular dichroism to study RNA folding transitions. *Methods Enzymol*, **317**, 393-409.
55. Borman, A.M., Bailly, J.L., Girard, M. and Kean, K.M. (1995) Picornavirus internal ribosome entry segments: comparison of translation efficiency and the requirements for optimal internal initiation of translation in vitro. *Nucleic Acids Res*, **23**, 3656-3663.
56. Lancaster, A.M., Jan, E. and Sarnow, P. (2006) Initiation factor-independent translation mediated by the hepatitis C virus internal ribosome entry site. *Rna*, **12**, 894-902.
57. Rijnbrand, R., Bredenbeek, P., van der Straaten, T., Whetter, L., Inchauspe, G., Lemon, S. and Spaan, W. (1995) Almost the entire 5' non-translated region of hepatitis C virus is required for cap-independent translation. *FEBS Lett*, **365**, 115-119.
58. Wang, C., Sarnow, P. and Siddiqui, A. (1994) A conserved helical element is essential for internal initiation of translation of hepatitis C virus RNA. *J Virol*, **68**, 7301-7307.

59. Varaklioti, A., Georgopoulou, U., Kakkanas, A., Psaridi, L., Serwe, M., Caselmann, W.H. and Mavromara, P. (1998) Mutational analysis of two unstructured domains of the 5' untranslated region of HCV RNA. *Biochem Biophys Res Commun*, **253**, 678-685.
60. Psaridi, L., Georgopoulou, U., Varaklioti, A. and Mavromara, P. (1999) Mutational analysis of a conserved tetraloop in the 5' untranslated region of hepatitis C virus identifies a novel RNA element essential for the internal ribosome entry site function. *FEBS Lett*, **453**, 49-53.
61. Forton, D.M., Karayiannis, P., Mahmud, N., Taylor-Robinson, S.D. and Thomas, H.C. (2004) Identification of unique hepatitis C virus quasispecies in the central nervous system and comparative analysis of internal translational efficiency of brain, liver, and serum variants. *J Virol*, **78**, 5170-5183.
62. Thelu, M.A., Drouet, E., Hilleret, M.N. and Zarski, J.P. (2004) Lack of clinical significance of variability in the internal ribosome entry site of hepatitis C virus. *J Med Virol*, **72**, 396-405.
63. Motazakker, M., Preikschat, P., Elliott, J., Smith, C.A., Mills, P.R., Oien, K., Spence, E., Elliott, R.M. and McCruden, E.A. (2007) Translation efficiencies of the 5'-untranslated region of genotypes 1a and 3a in hepatitis C infected patients. *J Med Virol*, **79**, 259-269.
64. Buratti, E., Gerotto, M., Pontisso, P., Alberti, A., Tisminetzky, S.G. and Baralle, F.E. (1997) In vivo translational efficiency of different hepatitis C virus 5'-UTRs. *FEBS Lett*, **411**, 275-280.
65. Lafuente, E., Ramos, R. and Martinez-Salas, E. (2002) Long-range RNA-RNA interactions between distant regions of the hepatitis C virus internal ribosome entry site element. *J Gen Virol*, **83**, 1113-1121.
66. Boehringer, D., Thermann, R., Ostareck-Lederer, A., Lewis, J.D. and Stark, H. (2005) Structure of the hepatitis C Virus IRES bound to the human 80S ribosome: remodeling of the HCV IRES. *Structure*, **13**, 1695-1706.

FIGURE LEGENDS

Figure 1. Translational activity of the natural HCV IRES variant isolated from clinical samples. (A). Schematic representation of the bicistronic constructs used. The HCV IRESes recovered from clinical samples were cloned into dual Luciferase bicistronic (DL) vectors harboring Renilla (RLuc) and Firefly (FLuc) luciferases as reporter genes. The 1b HCV IRES recovered from the HCV subgenomic replicon pFK-I_{377}neo/NS3-3'/wt (22), was cloned into a DL-vector to generate plasmid DL HCV-1b, the positive control. The RLuc/FLuc bicistronic vector harboring a defective encephalomyocarditis virus (ΔEMCV) IRES, named DL-ΔEMCV, known to inhibit ribosome reinitiation and readthrough, inserted upstream of the FLuc reporter was used as a negative control (25,26). (B) HCV IRESes arbitrarily numbered 1-28 isolated from clinical samples were cloned into the DL-vector. Viral genotype and number of recovered clones, number in brackets, are shown. Natural variations within the IRES nucleotide sequence were identified by sequencing followed by alignment with the 5'UTR of HCV genotype 1b (AJ238799.1), 2a (D00944), 3a (D17763) and 5a (Y13184) prototypes. DL-vectors were arbitrarily named according to their IRES, from 1 to 28 (IRES 1-28). Translational activity of the different DL RNAs with HCV-IRESes 1-28 were evaluated in comparison with the DL HCV-1b and the DL-ΔEMCV control RNAs in the RRL. RLuc and FLuc activities were measured and the [(FLuc/RLuc)] ratio was used as an index of IRES activity. The [(FLuc/RLuc)] ratio of the DL IRES-1b RNA was arbitrarily set at 100%. Values are the means +/- SD from three independent experiments.

Figure 2. Mutational analysis of the HCV 1b IRES. (A) The ability of the different 1b IRES mutants, named according to the mutation, to drive translation in the RRL was monitored. In these assays the FLuc/RLuc ratio was used as an index of IRES activity, with the mean translation efficiency of DL HCV-1b RNA being arbitrarily set at 100%. The HCV domains that harbor the mutations are indicated. Values are the means +/- SEM from three independent experiments. (B) Schematic depicting the secondary structure of the HCV IRES subdomain IIId showing the locations of the nucleotide mutations introduced into the HCV 1b IRES background. (C) The ability of the different 1b IRES mutants, named according to the mutation, to drive translation in the RRL (black bar) or in Huh-7 cell free translational extracts (white bars) programmed with *in vitro* synthesized RNA was monitored. In these assays the FLuc/RLuc ratio was used as an index of IRES activity, with the mean translation efficiency of DL HCV-1b RNA being arbitrarily set at 100%. Values are the means +/- SEM from three independent experiments. (D) Capped and polyadenylated RNA corresponding to the DL-vectors harboring the wt- or the IRES mutants were transfected into Huh-7 cell lines. Expression of the first cistron, RLuc, used as an indicator of transfection efficiency, and the expression from the second cistron, FLuc are shown. The FLuc/RLuc ratio was used as an index of IRES activity, with the mean translation efficiency of DL HCV-1b RNA being arbitrarily set at 100%. Values are the means +/- SD from three independent experiments.

Figure 3: Structural study of HCV IRES subdomain IIId. (A) Comparative structural analysis of the subdomain IIId wild type and mutant models. Superimposed structures taken at 0, 1, 2, 3, 4, 5 and 6 ns of the collection phase of MD simulations. The structures

are colored according to the average RMSD values. The main structural regions within subdomain IIId are mapped in the wild type model on left. Region I represents a right-handed A-form helix with Watson-Crick base pairing between nucleotides G253-C279, C254-G278 and C255-G277. Region II corresponds to a loop E structure with a characteristic S-turn composed of two sheared base pairs (G256-A276, A260-G273), a A257-A275 parallel base pair and a base triple between G258 and the reverse Hoogsteen pair U259-A274. Region III is a U262-G271 wobble base pair flanked by two Watson-Crick base pairs (G261-C272, G263-C270). Region IV is a disordered, -$_{264}$UUGGGU$_{269}$-, hexanucleotide (HN) loop region (20,51). (B) Average RMSD per nucleotide (computed for C3´ atoms) during 6ns of MD simulation. In the x-axis the HN loop bases appear highlighted in blue. Average RMSD values for the U265 base in the single mutant models are highlighted with an asterisk. (C) η-θ plot of nucleotide U265 during the MD simulation of; I) the HCV wt-IIId; II) the G266A-G268U double mutant; III) the G266A mutant and IV) the G268U mutant presented according to (36). (D) A representative MD snapshot of the *in silico* generated models (see text) in which the base stacking among the apical HN nucleotides is presented. The aromatic rings of nucleotides 264 to 269 appear in tubular form (licorice colored) according to the atom types. The remaining nucleotides are represented by lines. The green arrowhead indicates the additional hydrogen bond recognized during the simulation. (E) Stability of intramolecular hydrogen bond in the double mutant G266A-G268U monitored during the MD experiment. Distances between the heavy atoms of the hydrogen donor and acceptor groups are plotted. This interaction, together with the Watson-Crick G263-U270 base pair contributes to a decrease in the mobility of residues in the HN loop region.

Figure 4: HCV IRES subdomain IIId adopts an ion-dependent structure. (A) Circular dichroism spectra (CD) of synthetic 27-nt RNAs corresponding to nucleotides 253-279 of the wt-IIId upon thermal melting followed by renaturation in the presence of in varying concentrations (0, 1, 2, and 5 mM) of $MgCl_2$. Wavelength scans were recorded from 200 to 300 nm as indicated in Material and Methods. (B) Circular dichroism spectra (CD) of synthetic 27-nt RNA corresponding to nucleotides 253-279of the wt- and mutant IIId subdomains upon thermal melting followed by renaturation in the presence of 2 mM $MgCl_2$.

Figure 5: Wild type and the G266A/G268U double mutant HCV IRES subdomain IIId adopt similar ion-dependent structures. Circular dichroism spectra (CD) of synthetic 27-nt RNA corresponding to nucleotides 253-279 of the wt- or G266A/G268U double mutant-IIId upon thermal melting followed by renaturation in the presence of varying concentrations (A) 0, (B) 1 mM, (C) 2 mM, and (D) 5 mM of $MgCl_2$.

TABLE.

Table 1. Oligonucleotides used to generate the mutant HCV 1b IRESes described in this study.

Name	**orientation**	**Sequence (5' to 3')**
renFw	sense	TCGGACCCAGGATTCTTTTC
P2anti	antisense	TCTCTTCATAGCCTTATGCAGTTG
P1tag	sense	TGGCGAATAATTGGGGGCGACACTCCACCATAG
mut1	antisense	CGCCATGG**t**TAGACGCTTTC
mut2	antisense	TCCCGGGAGGGGGGG**g**CCT
mut3	antisense	CACTATGG**a**TCTCCCGGGAG
mut4	antisense	CGCCATGG**t**TAGACGCTTTC
mut5	antisense	CTACTCGGC**c**AGCAGTCTCG
mut6	antisense	TCGCGACC**t**AACACTACTCG
mut7	antisense	TCGCGA**a**CCAACACTACTCG
mut8	antisense	AAGGCCTTTCG**t**GACCCAAC
mut9	antisense	TGCACGGT**t**TACGAGACCTG
mut10	antisense	CTTTCG**t**GACCCAACACTACTCGGC**c**AGCAG
mut11	antisense	TCGCGA**a**C**t**AACACTACTCG

Mutations introduced in the HCV IRES are in lower case and in bold.

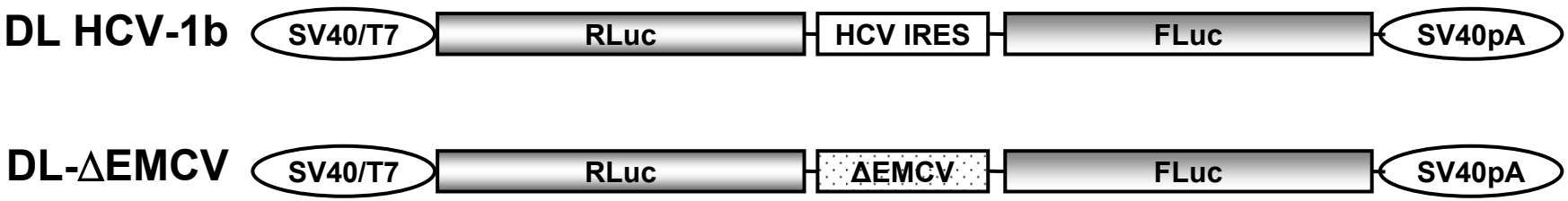
DL HCV-1b
SV40/T7
RLuc
HCV IRES
FLuc
SV40pA
DL-ΔEMCV
SV40/T7
RLuc
ΔEMCV
FLuc
SV40pA

Fig. 1A

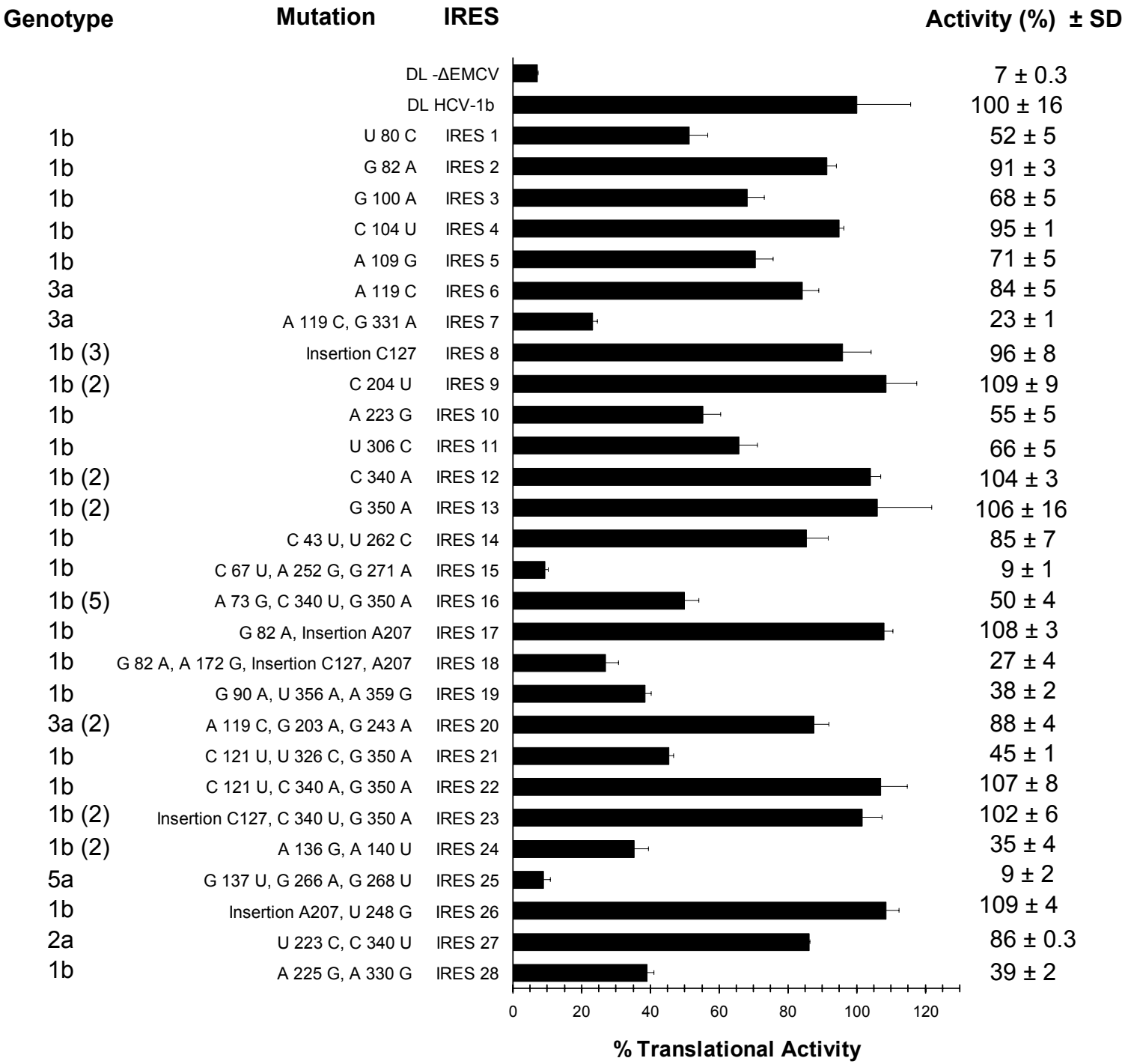
Genotype
Mutation
IRES
Activity (%) ± SD
DL -ΔEMCV 7 ± 0.3
DL HCV-1b 100 ± 16
1b U 80 C IRES 1 52 ± 5
1b G 82 A IRES 2 91 ± 3
1b G 100 A IRES 3 68 ± 5
1b C 104 U IRES 4 95 ± 1
1b A 109 G IRES 5 71 ± 5
3a A 119 C IRES 6 84 ± 5
3a A 119 C, G 331 A IRES 7 23 ± 1
1b (3) Insertion C127 IRES 8 96 ± 8
1b (2) C 204 U IRES 9 109 ± 9
1b A 223 G IRES 10 55 ± 5
1b U 306 C IRES 11 66 ± 5
1b (2) C 340 A IRES 12 104 ± 3
1b (2) G 350 A IRES 13 106 ± 16
1b C 43 U, U 262 C IRES 14 85 ± 7
1b C 67 U, A 252 G, G 271 A IRES 15 9 ± 1
1b (5) A 73 G, C 340 U, G 350 A IRES 16 50 ± 4
1b G 82 A, Insertion A207 IRES 17 108 ± 3
1b G 82 A, A 172 G, Insertion C127, A207 IRES 18 27 ± 4
1b G 90 A, U 356 A, A 359 G IRES 19 38 ± 2
3a (2) A 119 C, G 203 A, G 243 A IRES 20 88 ± 4
1b C 121 U, U 326 C, G 350 A IRES 21 45 ± 1
1b C 121 U, C 340 A, G 350 A IRES 22 107 ± 8
1b (2) Insertion C127, C 340 U, G 350 A IRES 23 102 ± 6
1b (2) A 136 G, A 140 U IRES 24 35 ± 4
5a G 137 U, G 266 A, G 268 U IRES 25 9 ± 2
1b Insertion A207, U 248 G IRES 26 109 ± 4
2a U 223 C, C 340 U IRES 27 86 ± 0.3
1b A 225 G, A 330 G IRES 28 39 ± 2
0
20
40
60
80
100
120
% Translational Activity

Fig. 1B

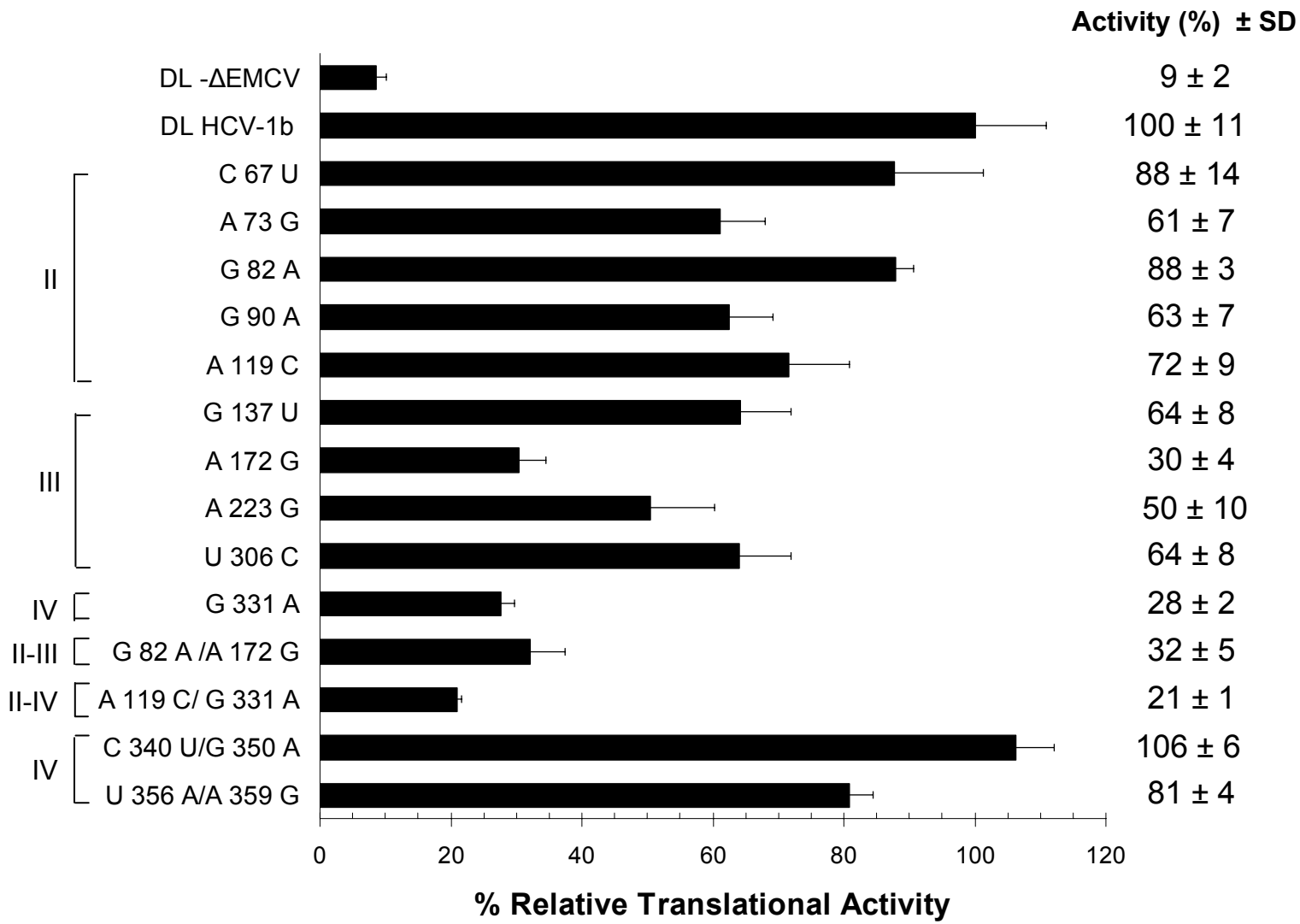
Activity (%) ± SD
DL -ΔEMCV
DL HCV-1b
C 67 U
A 73 G
G 82 A
G 90 A
A 119 C
G 137 U
A 172 G
A 223 G
U 306 C
G 331 A
G 82 A /A 172 G
A 119 C/ G 331 A
C 340 U/G 350 A
U 356 A/A 359 G
II
III
IV
II-III
II-IV
IV
9 ± 2
100 ± 11
88 ± 14
61 ± 7
88 ± 3
63 ± 7
72 ± 9
64 ± 8
30 ± 4
50 ± 10
64 ± 8
28 ± 2
32 ± 5
21 ± 1
106 ± 6
81 ± 4
0
20
40
60
80
100
120
% Relative Translational Activity

Fig. 2A

B

Mutation	Sequence
DL HCV-1b	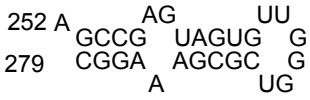
A 252 G	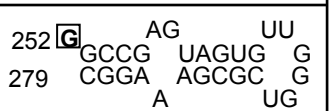
G 266 A	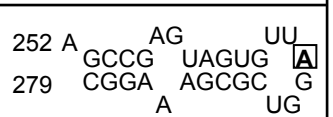
G 268 U	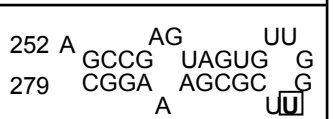
G 271 A	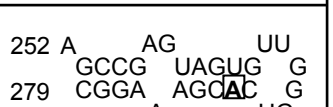
A 252 G/ G 271 A	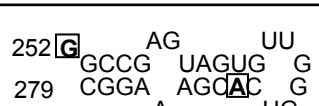
G 266 A/ G 268 U	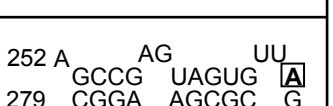

C

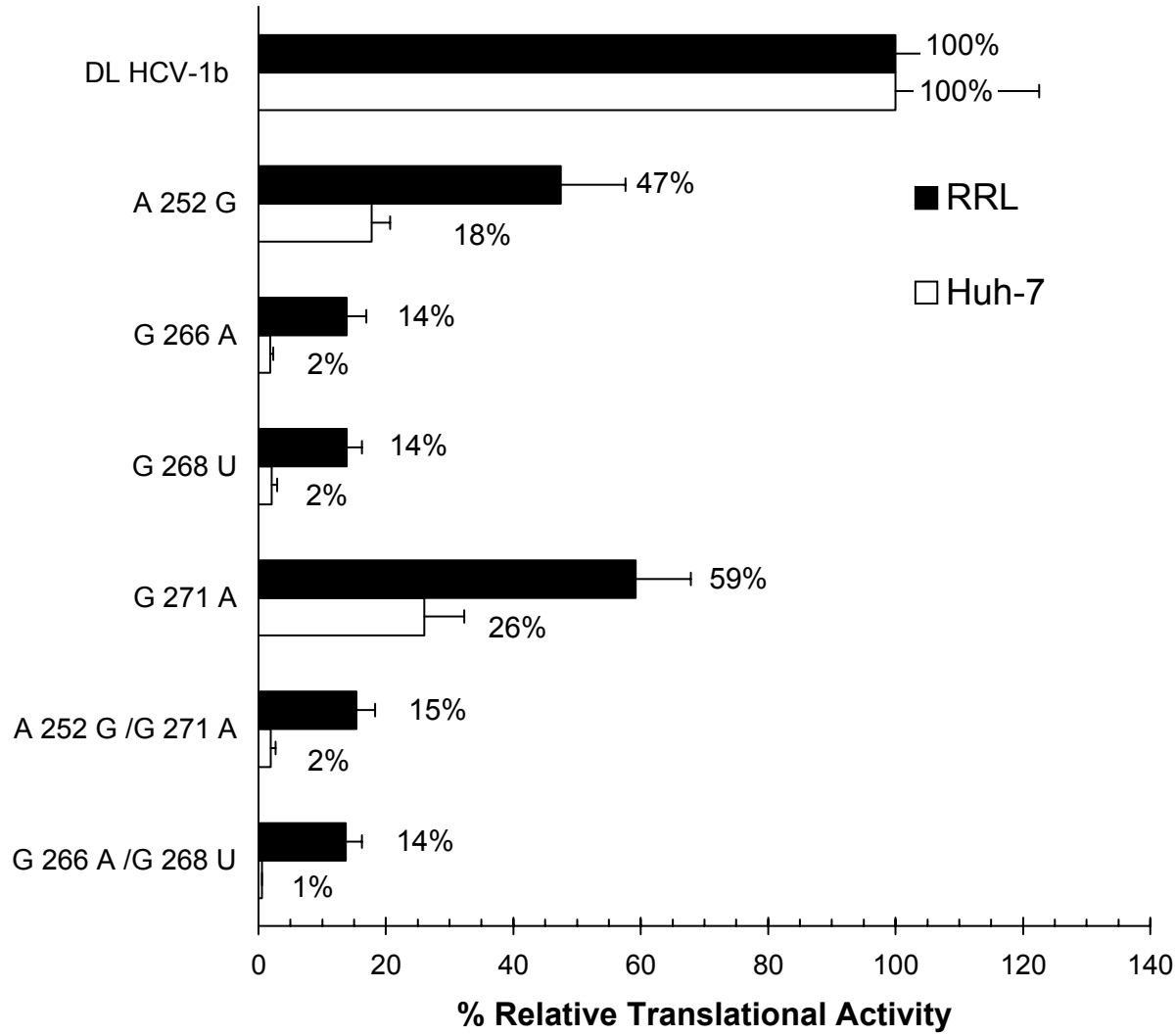

Fig. 2

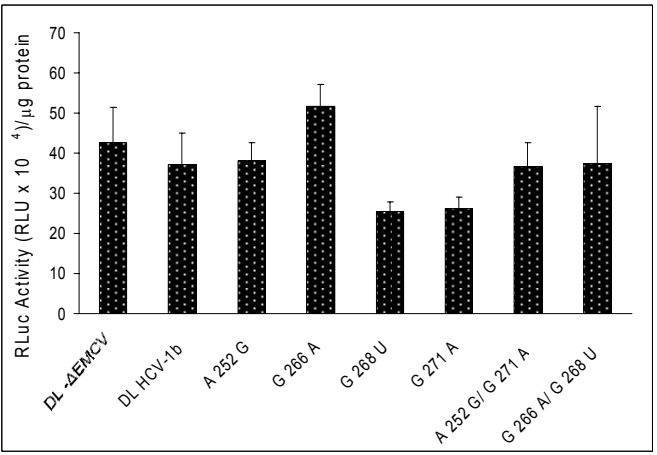
RLuc Activity (RLU x 10 ^{4})/μg protein
70
60
50
40
30
20
10
0
DL -ΔEMCV
DL HCV-1b
A 252 G
G 266 A
G 268 U
G 271 A
A 252 G/ G 271 A
G 266 A/ G 268 U

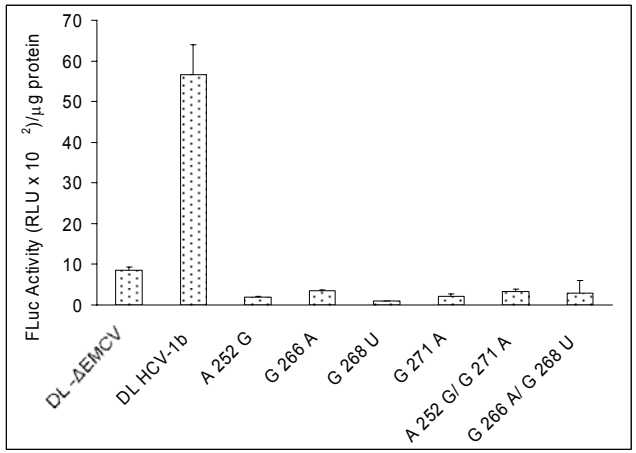
FLuc Activity (RLU x 10 ^{2})/μg protein
70
60
50
40
30
20
10
0
DL -ΔEMCV
DL HCV-1b
A 252 G
G 266 A
G 268 U
G 271 A
A 252 G/ G 271 A
G 266 A/ G 268 U

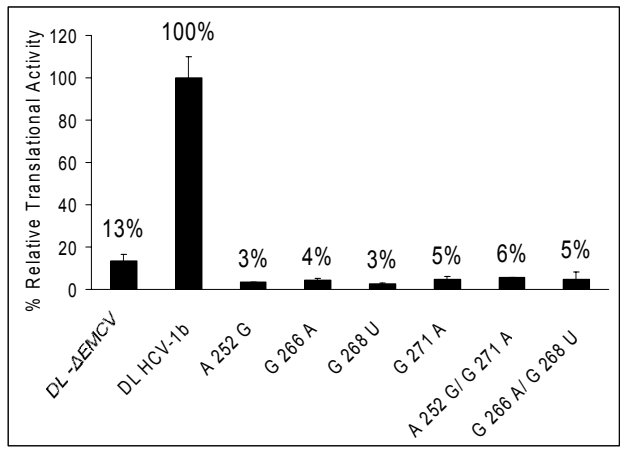
% Relative Translational Activity
120
100
80
60
40
20
0
100%
13%
3%
4%
3%
5%
6%
5%
DL -ΔEMCV
DL HCV-1b
A 252 G
G 266 A
G 268 U
G 271 A
A 252 G/ G 271 A
G 266 A/ G 268 U

Fig. 2D

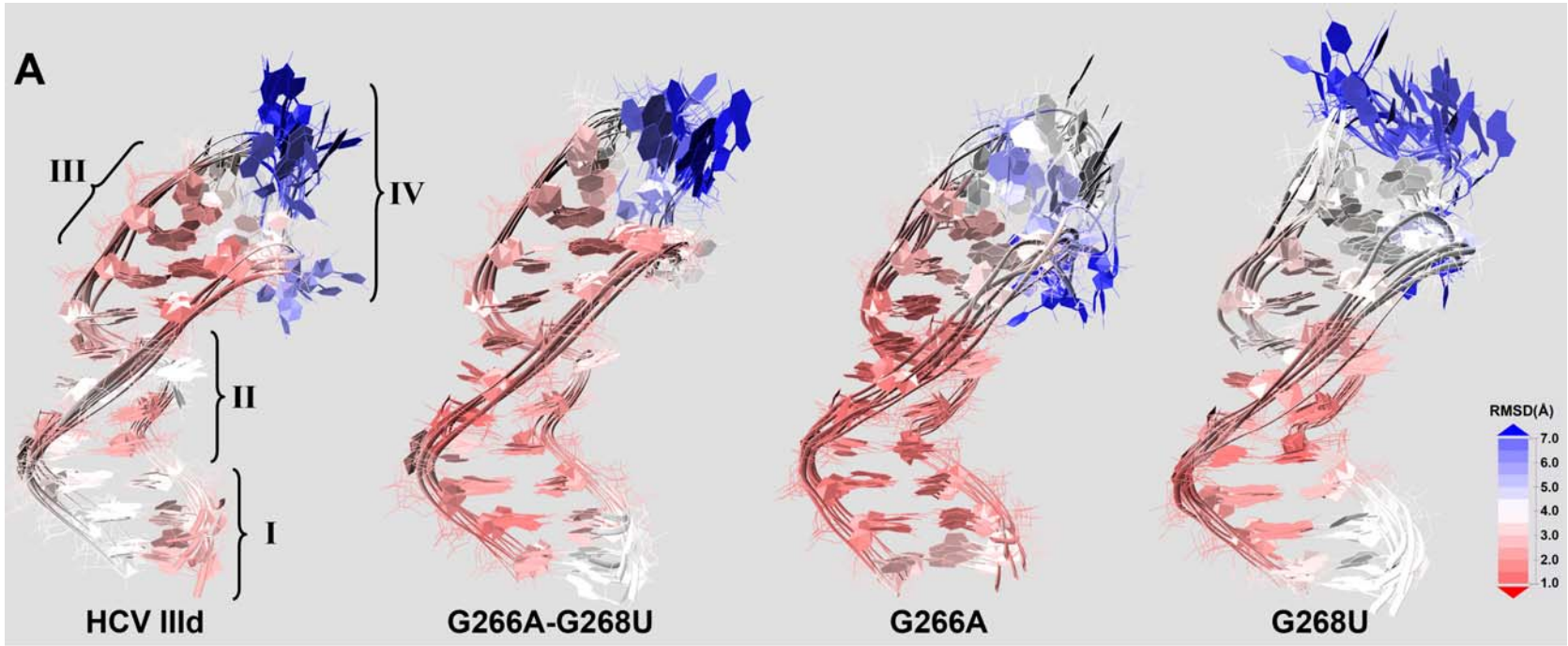
A
III
IV
II
I
HCV IIId
G266A-G268U
G266A
G268U
RMSD(Å)
7.0
6.0
5.0
4.0
3.0
2.0
1.0

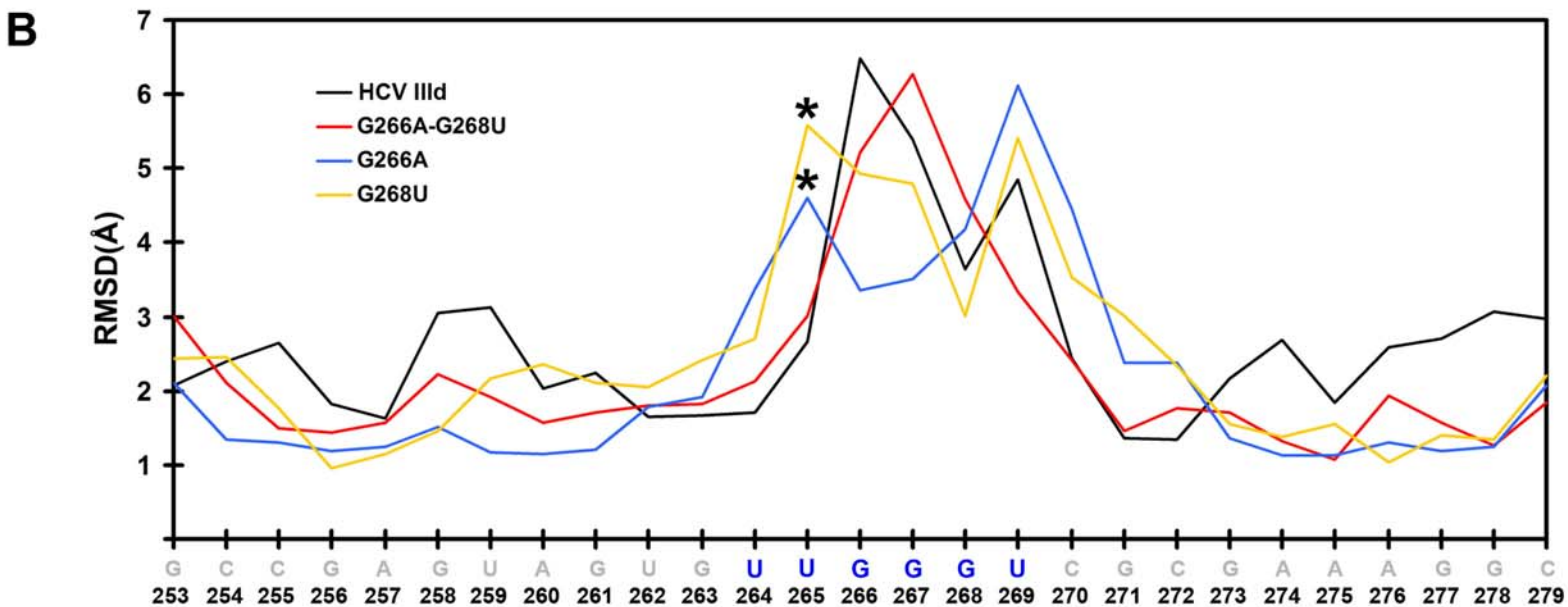
B
HCV IIId
G266A-G268U
G266A
G268U
RMSD(Å)
7
6
5
4
3
2
1
*
*
G C C G A G U A G U G U U G G G U C G C G A A A G G C
253 254 255 256 257 258 259 260 261 262 263 264 265 266 267 268 269 270 271 272 273 274 275 276 277 278 279

Fig. 3

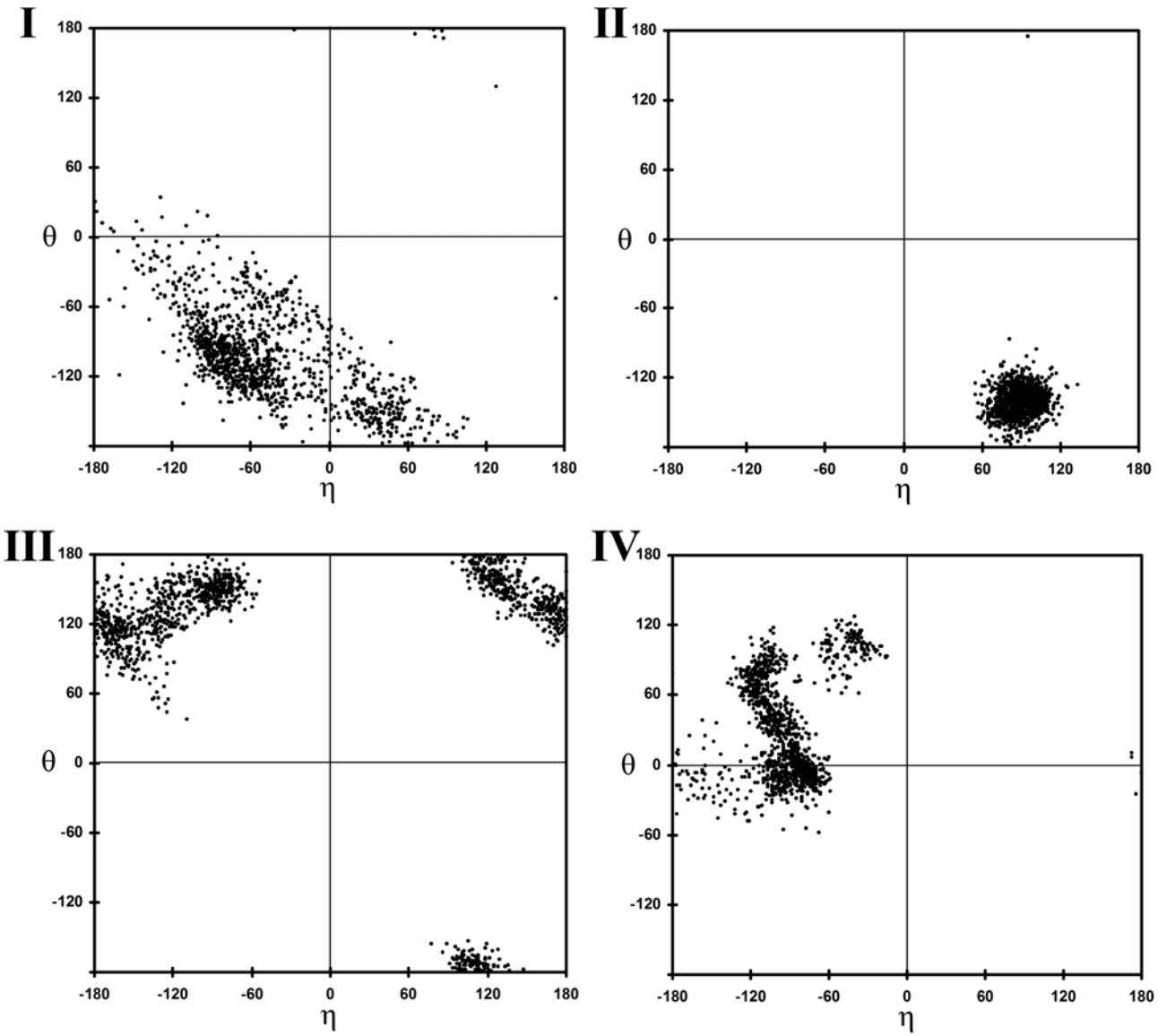

Fig. 3C

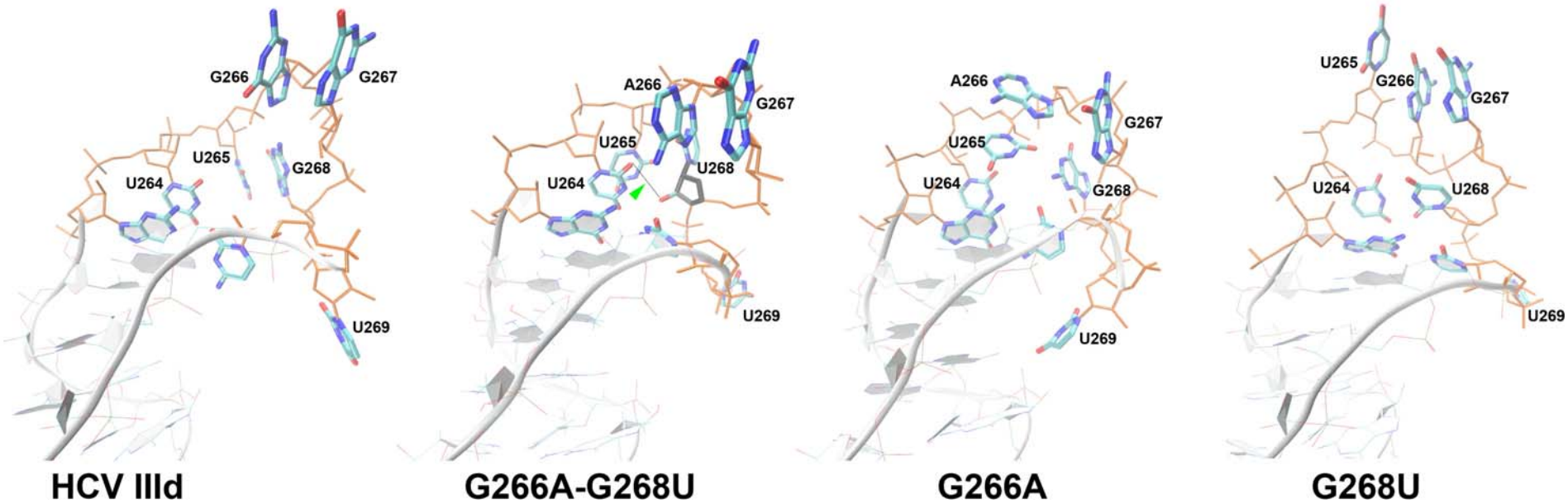
G266
G267
U265
G268
U264
U269
A266
G267
U265
U264
U268
U269
A266
G267
U265
U264
G268
U269
U265
G266
G267
U264
U268
U269
HCV IIId
G266A-G268U
G266A
G268U

Fig. 3D

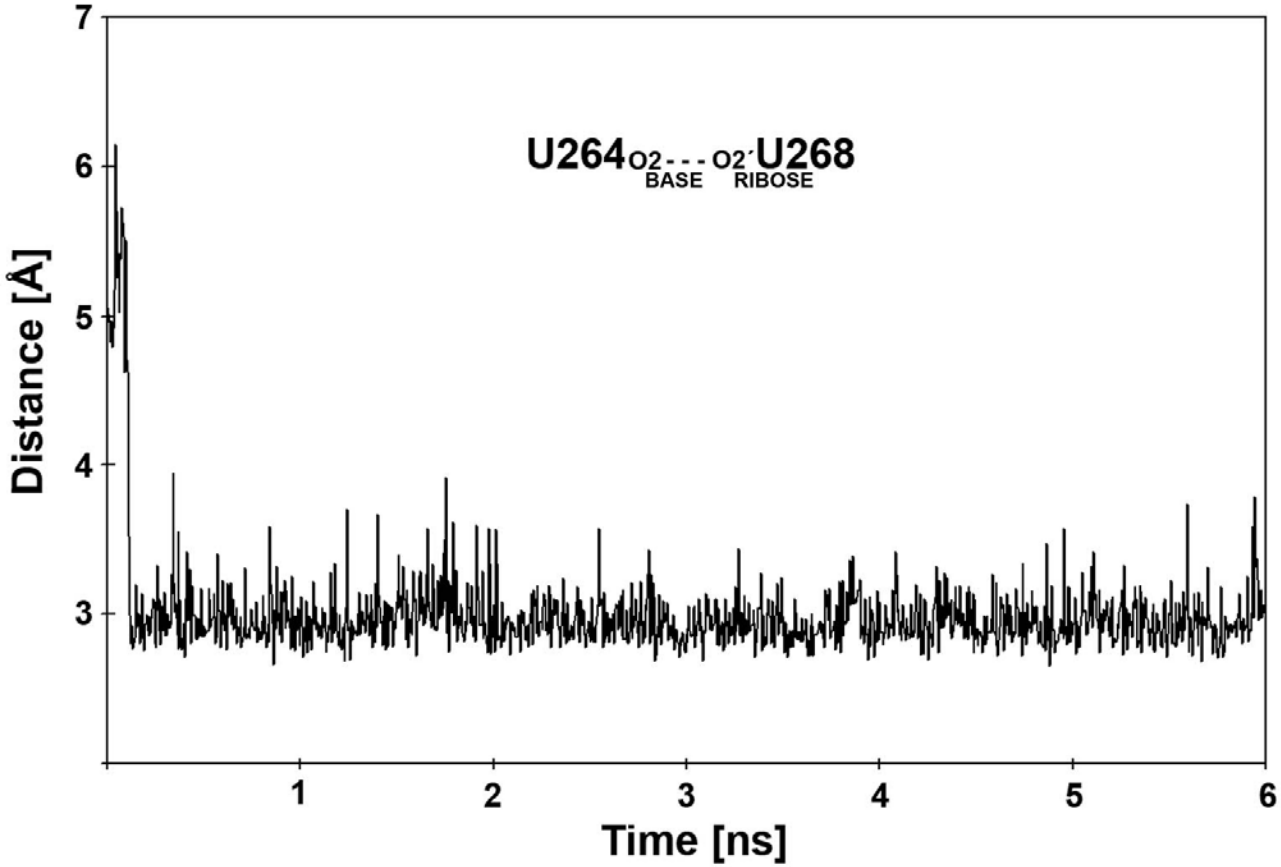

Fig. 3E

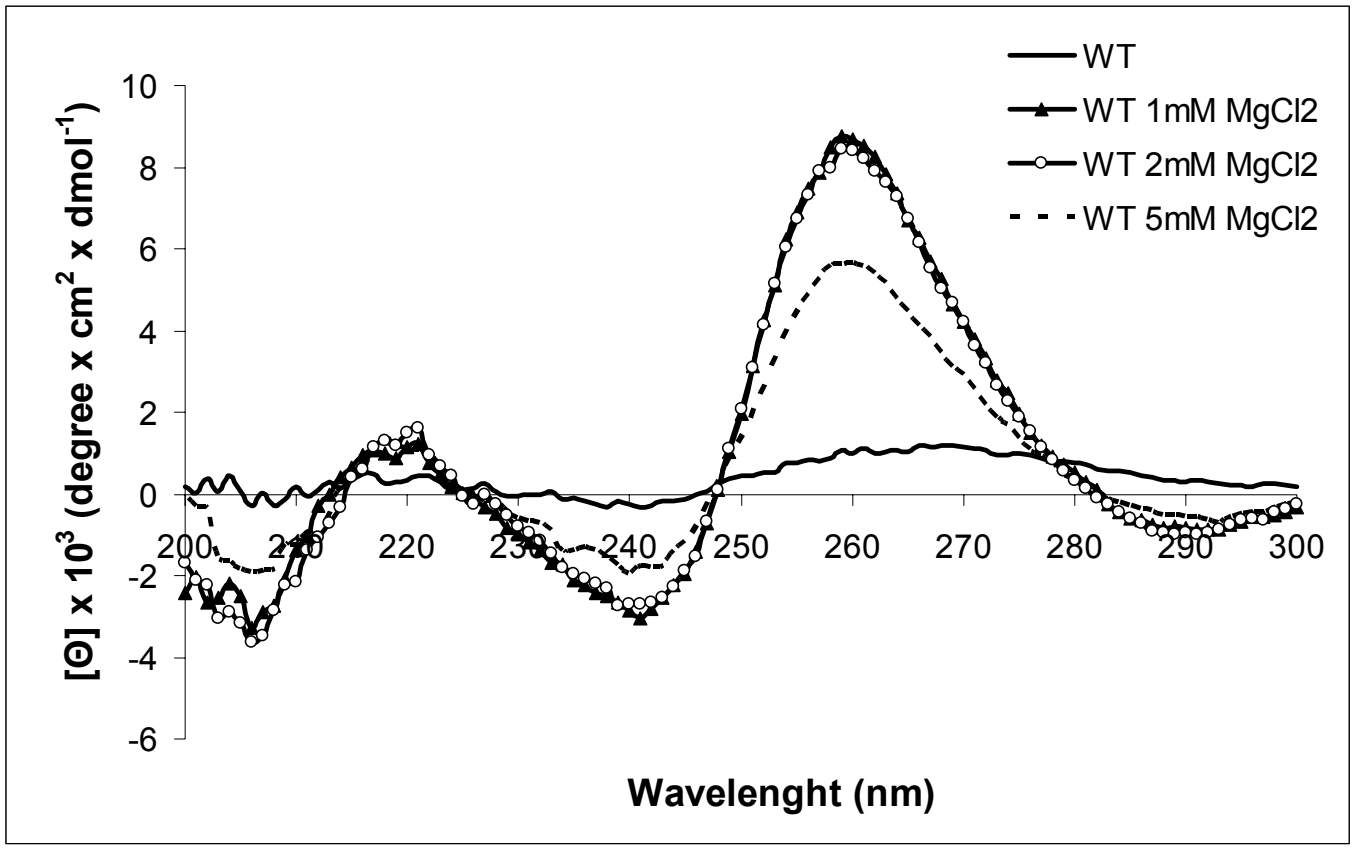
WT
WT 1mM MgCl2
WT 2mM MgCl2
WT 5mM MgCl2
[Θ] x 10^3 (degree x cm^2 x dmol^-1)
10
8
6
4
2
0
-2
-4
-6
200
220
240
250
260
270
280
290
300
Wavelenght (nm)

Fig. 4A

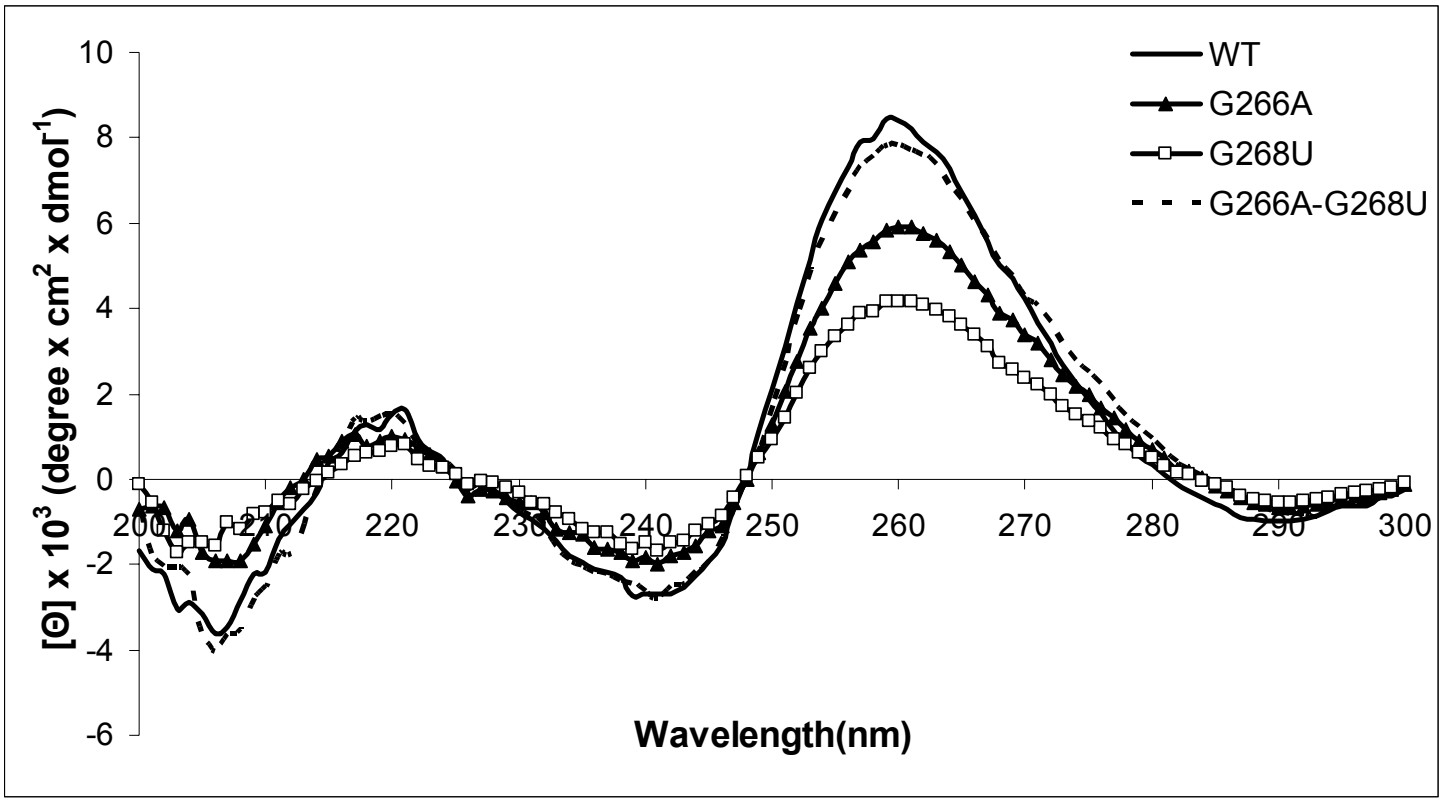
WT
G266A
G268U
G266A-G268U
[Θ] x 10^3 (degree x cm^2 x dmol^-1)
Wavelength(nm)
10
8
6
4
2
0
-2
-4
-6
200
210
220
230
240
250
260
270
280
290
300

Fig. 4B

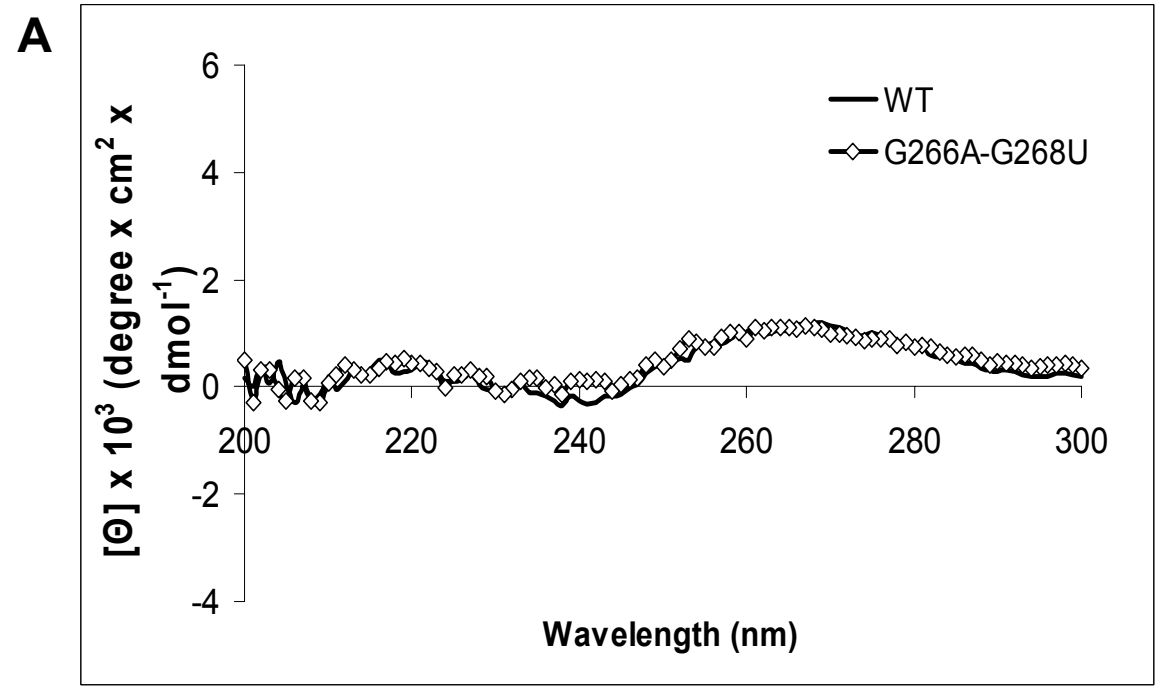
A
6
4
2
0
-2
-4
200
220
240
260
280
300
WT
G266A-G268U
[Θ] x 10^3 (degree x cm^2 x dmol^-1)
Wavelength (nm)

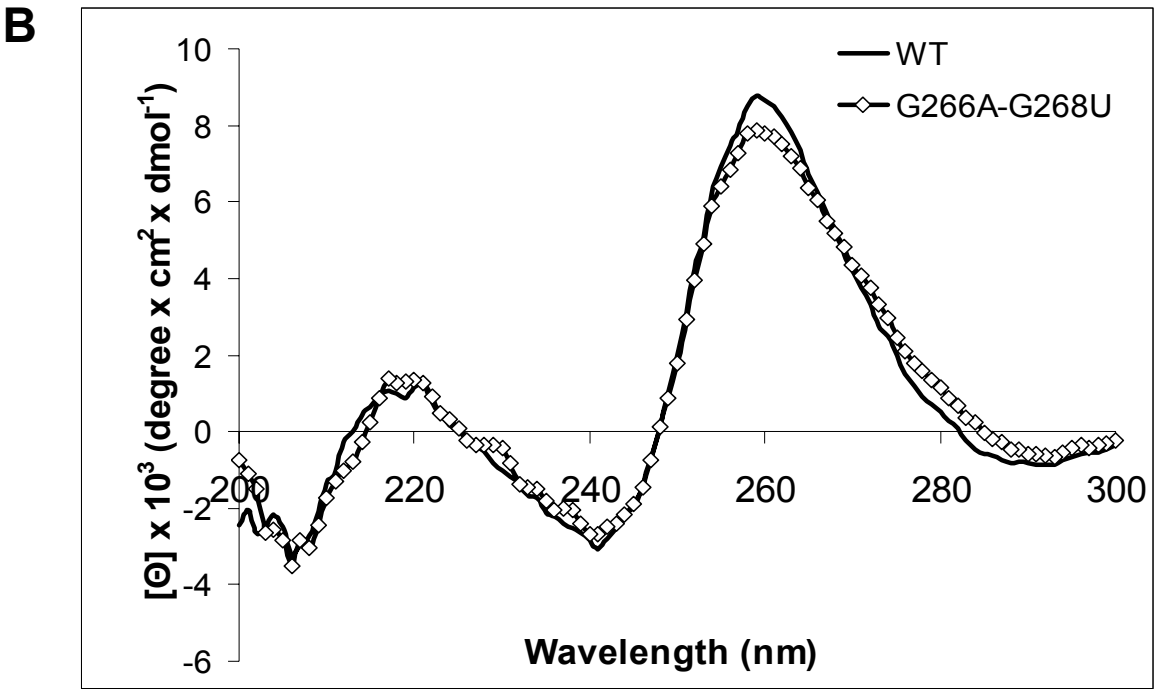
B
10
8
6
4
2
0
-2
-4
-6
200
220
240
260
280
300
WT
G266A-G268U
[Θ] x 10^3 (degree x cm^2 x dmol^-1)
Wavelength (nm)

Fig. 5

C

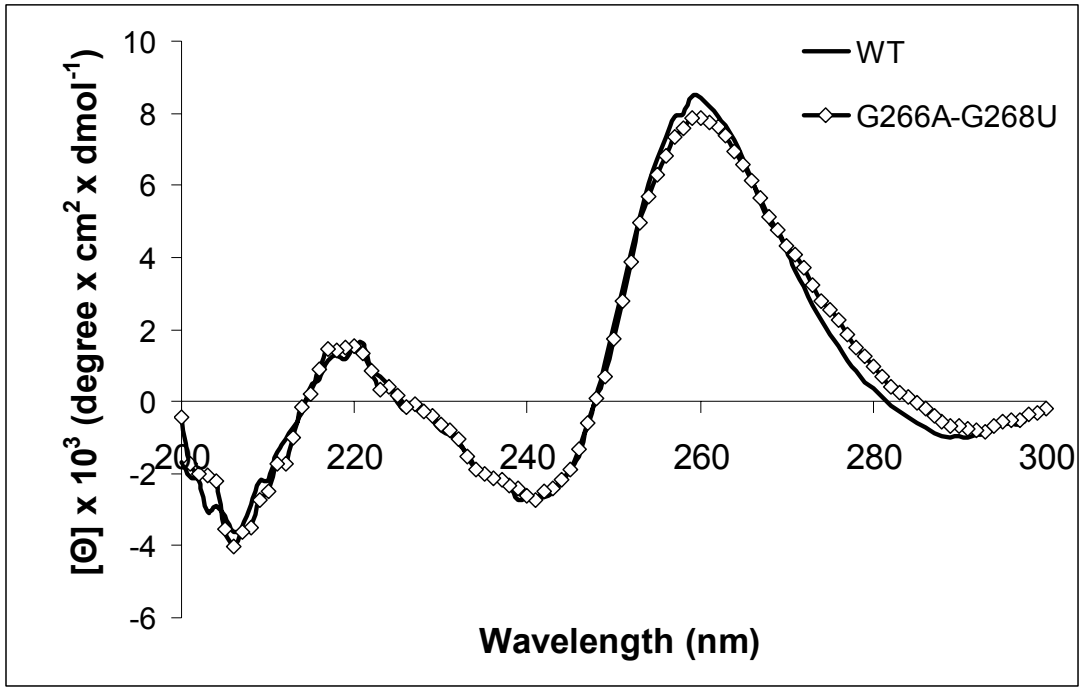
WT
G266A-G268U
[Θ] x 10^3 (degree x cm^2 x dmol^-1)
10
8
6
4
2
0
-2
-4
-6
200
220
240
260
280
300
Wavelength (nm)

D

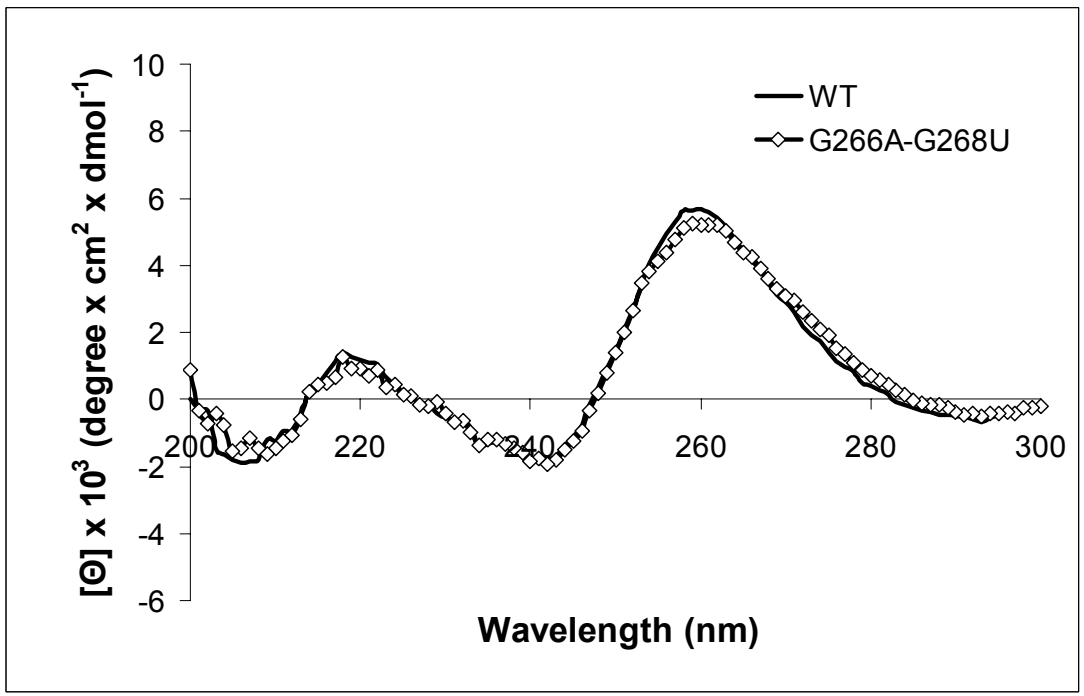
WT
G266A-G268U
[Θ] x 10^3 (degree x cm^2 x dmol^-1)
10
8
6
4
2
0
-2
-4
-6
200
220
240
260
280
300
Wavelength (nm)

Fig. 5